Title

Molecular Dynamics Simulations of Rhodamine B Zwitterion Diffusion in Polyelectrolyte Solutions.

Journal

The Journal of Physical Chemistry B: Biophysical Chemistry, Biomaterials, Liquids, and Soft Matter, 126(48)

Authors

Walhout, Peter
He, Zhe
Nawrocki, Grzegorz
et al.

Publication Date

2022-12-08

DOI

10.1021/acs.jpcb.2c06281

Peer reviewed

HHS Public Access

Author manuscript

J Phys Chem B. Author manuscript; available in PMC 2023 December 08.

Published in final edited form as:

J Phys Chem B. 2022 December 08; 126(48): 10256–10272. doi:10.1021/acs.jpcb.2c06281.

Molecular Dynamics Simulations of Rhodamine B Zwitterion Diffusion in Polyelectrolyte Solutions

Peter K. Walhout[*],
Wheaton College, Chemistry Department, 501 College Ave, Wheaton, IL 60187

Zhe He,
Wheaton College, Chemistry Department, 501 College Ave, Wheaton, IL 60187

Bercem Dutagaci,
Michigan State University, Biochemistry and Molecular Biology, 603 Wilson Road, Room 218, East Lansing, MI 48824

Grzegorz Nawrocki,
Michigan State University, Biochemistry and Molecular Biology, 603 Wilson Road, Room 218, East Lansing, MI 48824

Michael Feig
Michigan State University, Biochemistry and Molecular Biology, 603 Wilson Road, Room 218, East Lansing, MI 48824

Abstract

Polyelectrolytes continue to find wide interest and application in science and engineering, including areas such as water purification, drug delivery, and multilayer thin films. We have been interested in the dynamics of small molecules in a variety of polyelectrolyte (PE) environments, and in this paper we report simulations and analysis of the small dye molecule, rhodamine B (RB), in several very simple polyelectrolyte solutions. Translational diffusion of the RB zwitterion has been measured in fully atomistic, 1-μs long molecular dynamics simulations in four different polyelectrolyte solutions. Two solutions contain the common polyanion sodium poly(styrene sulfonate) (PSS), one with a 30-mer chain, the other with 10 trimers. The other two solutions contain the common polycation poly(allyldimethylammonium) chloride (PDDA), one with two 15-mers, the other with 10 trimers. RB diffusion was also simulated in several polymer-free solutions to verify its known experimental value for the translational diffusion coefficient, D_{RB}, of 4.7×10^{-6} cm^2/s at 300 K. RB diffusion was slowed in all four simulated PE solutions, but to varying degrees. D_{RB} values of 4.2×10^{-6} and 3.6×10^{-6} cm^2/s were found in PSS 30-mer and PSS trimer solutions, respectively, while PDDA 15-mer and trimer solutions yielded values of 2.1×10^{-6} and 3.9×10^{-6} cm^2/s. Significant associations between RB and the PEs were analyzed and interpreted via a two-state diffusion model (bound and free diffusion) that describes the data well.

[*] peter.walhout@wheaton.edu, Phone:630-752-5404.

Supporting Information Available: partial charges, force-field parameters, analysis of polymer structure and diffusion, comparison of RB tracer diffusion in dilute polymer solutions with previous theory and experiment, additional histograms describing RB contacts in all four PE systems, potential of mean force curves.

Crowder size effects and anomalous diffusion were also analyzed. Finally, RB translation along the polyelectrolytes during association was characterized.

Graphical Abstract

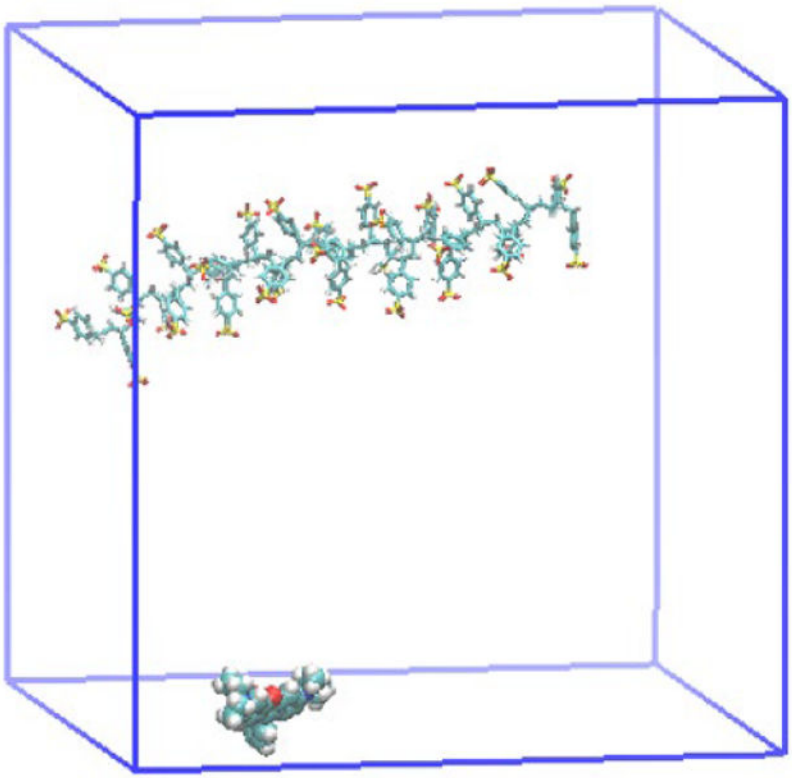

1. Introduction

Scientists have studied polyelectrolytes (PEs) experimentally and theoretically for about as long as macromolecules and ions have been understood to exist. After the discovery of their intrinsic properties, PEs became important additives in soaps, cosmetics, and foods. These properties include their water solubility, strong intra- and inter-chain interactions, ionic conductivity, and surface activity.[1] Given their widespread prevalence in the natural world and their unique properties, it is little wonder that the study of PEs continues unabated in the physical and life sciences. While a great deal of recent research attention has focused on PE multilayer thin films[2–8] and complexes,[9–11] which involve two oppositely charged PEs, and on the use of polymeric ionic liquids for use in batteries and other applications,[12–15] PE solutions continue to attract attention, as well.

This paper focuses on tracer diffusion in various dilute PE solutions, examining both polycation and polyanion solutions. While small molecule tracer diffusion has a long history in polymer and PE research,[16] it remains an ongoing area of research. Not only is such work still important as a probe of polymer dynamics, but many applications involve PE interactions with small molecules. Dyes mixed with macromolecules for fabric coloring is

perhaps the most obvious and oldest area of applied interest in this area, but recent interest in dilute and semi-dilute solutions has included potential uses in drug and protein delivery and the controlled release of entrapped molecules,[17] the use of PEs in waste water treatment of textile plants,[18–20] where dye removal from the waste stream is important for both safety and dye recovery, solution-based selective colormetric sensors for various ions,[21–24] dye uptake by PE-micelle coacervates,[25] and using dyes to control the coacervation and precipitation of oppositely charged PEs in solution.[20] Finally, the specific PEs studied here, poly(styrene sulfonate) (PSS) and poly(diallydimethylammonium) chloride (PDDA) (Figure 1), are commercially significant in their own right and have been widely studied and characterized, e.g. PSS is used in ion-exchange resins and treatment of hyperkalemia,[26] while PDDA is widely used in water treatment and the paper industry, and is regarded as a model for polyelectrolyte behavior.[27,28]

In addition to helping develop specific applications, investigations of small molecule diffusion in PE solutions continue to explore conceptual and theoretical aspects of these surprisingly complex systems. Even in dilute and semi-dilute solutions, which are free from polymer entanglements and are relatively well understood relative to concentrated solutions and PE melts, there are still areas of active research. Recently, for instance, nanoparticles were found to be unexpectedly sub-diffusive due to confinement in a PSS solution that was dilute enough to have no entanglements.[29,30] There are also a variety of ways to fit diffusion data in PE solutions, with no one-size-fits-all approach.[31–37] The role of counterions in PE solution dynamics, typified by the decades-long exploration of the Hoffmeister series and its role in protein and other PE structures and dynamics,[38–40] also continues to be the subject of investigation, even apart from any role they play in diffusion.[41–49] Computer simulations are essential for fully testing theories of counterion condensation and their predictions of radial distribution functions. Finally, the role of PEs as crowders in technological and cellular diffusive processes are also under active investigation, including elucidating the combined effects of attractions and crowding.[50–53]

The small molecule in this study, Rhodamine B (RB, Figure 1), is a popular tracer dye and biological stain due to its strong absorbance and intense fluorescence. Rivas et al. have studied RB interactions with PSS in solution, finding the fluorescent properties are changed based on association with the charged polymer, but also as a function of the solution pH.[54] They observe that under pH = 5, when the zwitterion of RB is being protonated to give it a full positive charge and great attraction to the oppositely charged PSS, the effects on fluorescence are strongest. However, they speculate that the RB zwitterion at pH > 5 has little to no binding with PSS. The simulation results presented here show, perhaps unexpectedly, that even in dilute solution the RB spends a significant amount of time bound to PSS (as well as to PDDA in PDDA solutions).

Given that diffusion is involved at some level in nearly all physical and chemical processes, there is a rich literature for many types of systems. The study of diffusion in crowded systems and the understanding of anomalous diffusion has grown substantially in the last two decades as investigative methods such as fluorescence correlation spectroscopy (FCS) and various computer simulations have matured.[55–74] Theoretical clarity has also developed regarding important related concepts such as non-Gaussian particle distribution

functions,[63,64,74,75] ergodicity breaking,[65,66,73] and aging.[76,77] Relevant to the simulations presented in this paper is experimental work by Jia et al. who used FCS to study both cationic and anionic forms of rhodamine 6G (R6G) in PSS solutions.[45] While the majority of the cationic R6G was bound to the negative polyanion PSS and FCS autocorrelations were fit to a two-component diffusion model, the anionic R6G remained free and exhibited diffusion comparable to that in polymer-free water. Such anomalous diffusion has been observed in many systems, and is the main focus of several studies.[55,61,68–71] However, the specific interactions between small molecule diffusers and polymer chains that lead to slower and anomalous diffusion are difficult to discern experimentally, making computer simulations an attractive corollary for revealing these details.

In the last three decades, computer technology and simulation methodologies have progressed to the point where molecular dynamics (MD) and Monte Carlo (MC) simulations of PEs and their solutions are now not just feasible but increasingly able to provide new insights that are complementary to experiment. An increasing number of simulation studies of various PE solutions have been performed in the last decade,[35,41,78–87] using both all-atom (AA) and coarse-grained models for both MD and Monte Carlo methods. Holm and co-workers have studied PDDA and PSS specifically.[84–87] Of all these simulations, Vagias et al. is perhaps most relevant to the work reported herein, as they used both experimental FCS and computer simulation to study small molecule diffusion in aqueous solutions of a terpolymer consisting mostly of *N*-isopropyl acrylamide.[35] This study, which utilized a variety of small molecule tracers, including R6G, examined the effects of polymer concentration and tracer/polymer attraction on diffusion. While the systems with strong attractions demonstrated anomalous diffusion, it was clear a two-component diffusion model consisting of free diffusion and bound diffusion could explain the observed data. The simulation utilized a generic bead-spring model and implicit solvent.

We present here fully atomistic MD simulations of RB diffusion in a variety of dilute aqueous PSS and PDDA solutions. The attraction of a zwitterion and a PE is not one that is easily understood or predicted apart from the molecular details of a fully atomistic simulation; it lacks the obvious electrostatic repulsion or attraction of an ionic dye to a PE, as in the Jia et al or Vagias et al. studies. Yet, we find there is clear on/off binding of RB, and on a time scale that can easily be tracked in a 1 μs simulation. While there have been a few simulation studies of small molecule tracer diffusion in polymer systems, these are the first fully atomistic simulations of small molecule diffusion in PE solutions. We report detailed explorations of the polymer conformation and diffusion, as well as RB diffusion and association dynamics between the RB zwitterion and the various PEs. To further explore the role that molecular crowding possibly plays in this system apart from any attractive interactions, we also broke up each of the two PEs into solutions of trimers with virtually equal concentrations and volume fractions and observed how the RB diffused among the smaller, more mobile PE obstacles.

We find interesting variations in the RB diffusion due to various levels of RB/PE association in the four different systems. Free and bound states of RB are clearly identified and well-sampled during the simulated trajectories in all four systems, so a multi-state diffusion model is justified,[65] allowing the unusual variation of RB diffusion to be explained quite

simply. Such a multi-state approach is common in modeling diffusion in dilute and semi-dilute solutions.[35,45,60,65,88,89] Additionally, we find evidence for dimeric associations of PSS trimers that is not present for PDDA, which also affects the RB diffusion. It is speculated this may result from the far greater condensation of the sodium counterions on the PSS compared to the chloride ions with PDDA. We also elucidate in atomic detail the nature of the RB/PE binding attractions, including unexpected RB mobility up and down a PE chain during a binding event.

Finally, this study was partly motivated by the experimental observation of complex diffusion dynamics of RB on the surface of a PEM thin film,[90,91] where the outermost region of a water-immersed PEM can consist of single PE chains dangling into solution, similar to a dilute or semi-dilute PE solution. The observation here of regular attachment and detachment of RB to both PSS and PDDA thus informs small molecule behavior at the water-swollen surface of PEMs and also at the surface of PE brushes, where similar complex diffusion has been observed experimentally.[92,93]

2. Methods

2.1. Molecular Dynamics Simulations

The structures of the RB zwitterion, and of PSS polyanion and PDDA polycation oligomers, were initially constructed and optimized in vacuum using the AM1 semi-empirical method to obtain the partial charges used in the simulations (see Supplementary Information for all partial charges). The bonded parameters of PSS, PDDA, and RB are based on the general AMBER force field (GAFF), and were generated in CHARMM format through the ACPYPE website (see Supplementary Information for complete force-field parameters).[94–96] Lenard-Jones parameters were also taken from GAFF. CHARMM, together with OpenMM,[97] was the molecular dynamics software package used to perform the simulations.[98] The input files of all the polyelectrolytes were assembled in CHARMM using the force fields and structures of the end groups and one type of repeating unit and then equilibrated in vacuum. The partial charges of the one repeating unit were based on an average of the middle groups in the AM1 oligomers. The bond lengths involving hydrogen atoms were constrained using the SHAKE algorithm. All the polyelectrolytes used for our simulations are isotactic. For PDDA, because the ring attaches at two chiral centers to the carbon chain backbone, there are both *cis* and *trans* conformations; we have simulated the lower energy *trans* isotactic conformation. The RB zwitterion has a negative charge largely centered on the carboxylate, but the positive charge is delocalized over the entire ring system.

Prior to all the simulations of RB in polymer solutions, the end-to-end distance of the PSS and PDDA in 100 mM NaCl solution were examined in various sizes of periodic boxes in order to determine the ideal box size. In general, a box size with an edge length between 70 and 90 Å was considered ideal; it is big enough to keep the polyelectrolyte chain isolated from its periodic images, while still small enough to minimize the number of water molecules in the system, enabling us to finish the 1 μs simulations within a reasonable amount of time.

The various simulated systems are described in Table 1 and depicted in Figure 2. PEs and RB were randomly positioned in a cubic box with periodic boundary conditions (PBC) and solvated with TIP3P water molecules. PSS and PDDA were neutralized by counterions (Na^+ and Cl^-). These systems were NVT equilibrated for 6 ps sequentially at 50, 150, 250, and 300 K, followed by 300 ps of NPT equilibration at 300 K and 1 atm. (All NPT equilibration runs were carefully monitored for energy and volume equilibration before a production run was started.) All the product simulations were performed on GPUs with CUDA using CHARMM/OpenMM. The Berendsen coupling scheme was used for temperature control with a coupling time constant for temperature of 0.1 ps. The cutoff distance for the Lennard-Jones and direct-space electrostatic interactions was set at 12 Å. Each system was simulated using a timestep of 2 fs, and the trajectory snapshots were saved every 10 ps. Long-range electrostatic interactions were treated using the Particle Mesh Ewald (PME) method.[99]

Benchmark simulations for RB diffusion were performed using systems containing water, RB and varying amounts of NaCl. Details of these polymer-free simulations are listed in Table 2.

2.2. Analysis

The primary analysis accomplished in these MD simulations is the calculation of the translational diffusion coefficients, D, for PDDA, PSS, and RB. We first extract the mean square displacement (MSD) of the molecular center of mass, defined as

$$\mathrm{MSD}(\tau) = \langle (\vec{r}(t+\tau) - \vec{r}(t))^2 \rangle \quad (1)$$

where $\vec{r}$ is the time-dependent position of the molecule, and $\boldsymbol{\tau}$ is the time lag between two positions. MSD($\boldsymbol{\tau}$) is thus an average for a given $\boldsymbol{\tau}$ over the entire duration of the simulation, i.e. from t = 0 to (1 μs – $\boldsymbol{\tau}$). MSD vs. time is quite linear on 2–100 ns timescales (Figure 3). The slope of the line is used to determine D via the standard solution of the three-dimensional diffusion equation:

$$\mathrm{MSD} = 6D\tau \quad (2)$$

To avoid poor statistics, only the first 20 ns of each 1 μs MSD was fit, i.e. 2% of the entire length of the trajectories. In addition, the first 2 ns were eliminated to avoid non-linearity from early-time anomalous diffusion. The D values taken directly from the linear fits of the MSDs we term D_{MD}. For the split MSDs, which separately characterize bound and unbound RB diffusion within one simulation run, data was fit out to 10% of each MSD, since 2% of these much shorter trajectories were often less than 2 ns. Additionally, the MSDs for the unbound RB were so short that we eliminated only the first 0.2 ns from the fitting, but this is justified given the lack of anomalous RB diffusion in PE-free water.

Two standard corrections to any value of D_{MD} need to be made before comparing with typical ambient experimental conditions. First, there is a correction due to altered hydrodynamic diffusion in finite-size periodic systems. The PBC correction as a function of the cubic simulation box edge length, E, is given by eq 3:[100,101]

$$D_{\mathrm{MD}} + \frac{kT\xi_{\mathrm{EW}}}{6\pi\eta E}\alpha = D_{0,\,\mathrm{TIP3P}} \tag{3}$$

where $D_{0,\mathrm{TIP3P}}$ is the diffusion coefficient in the limit of an infinite-sized box that would correspond to experiments without PBC at the given temperature T and solution viscosity, η. ξ_{EW} is the theoretical correction factor for cubic simulation boxes in a simulation employing an Ewald summation and is equal to 2.8373.[101] The final α is an empirical factor used for larger molecules instead of point diffusers (for which $\alpha = 1$), and has been found to be equal to 0.76 for RNA oligomers.[101] (We use the same value of 0.76 for RB, given its comparable size to the trinucleotide whose diffusion generated this α value.) The viscosity used for $D_{0,\mathrm{TIP3P}}$ is the viscosity of TIP3P water at 300 K and 1 bar, which is 3.06×10^{-4} kg m^{-1} s^{-1}, obtained by interpolating the data of Venable et al.[102]

The second correction needed is a standard compensation for the simulated TIP3P water viscosity, which is too low.[102,103] This viscosity scaling, which is valid for even moderately concentrated solutions, is roughly a factor of 3, due to TIP3P water having $\eta = \sim 3 \times 10^{-4}$ kg m^{-1}s^{-1} at ambient conditions, whereas ambient aqueous solutions have $\eta = \sim 9 \times 10^{-4}$ kg m^{-1} s^{-1}. The precise viscosity of pure water at 300K and 1 bar is 8.55×10^{-4} kg m^{-1}s^{-1} according to interpolating the given experimental data in Venable et al. Multiplying $D_{0,\mathrm{TIP3P}}$ by a viscosity scaling factor of 3.06/8.55 = 0.358 thus yields D_0, which is the value that can be compared directly to experimental values. TIP3P remains one of the most used water models in simulations,[104,105] especially in biomolecular simulation, so this viscosity scaling is standard procedure and continues to yield good diffusion results compared to experiment.

Other properties analyzed here include the root-mean-square distance between polymer chain ends, r_{rms},[106] the radius of gyration, $R_{\mathrm{g,rms}}$, which is the square root of the weight-averaged value of r_{i}^2, where r_{i} is the distance of the i^{th} atom from the molecular center-of-mass, and the solvent accessible surface area (SASA). SASA was computed and averaged for several random configurations of the production run using the “rolling ball” algorithm developed by Shrake and Rupley after the original idea of Lee and Richards.[107,108] The probe radius used is the typical value of 1.4 Å to model a water molecule. This is significantly smaller than the length of a repeating unit of polyelectrolyte (3–5 Å). We have also computed radial distribution functions to elucidate various pair correlations in the simulations. All these analyses were accomplished using MMTSB (Multiscale Modeling Tools for Structural Biology)[109] in combination with CHARMM.[98]

To better explore attractive associations between RB and the polymers, we defined a contact distance by analyzing their time-dependent separation over the course of the simulations. Figure 4 clearly depicts the on/off nature of the RB association with both PDDA and PSS. The closest distance between a heavy atom (non-hydrogen) of RB and a heavy atom of the PE is plotted over the duration of run 1 for both long chain PEs. From this, we define contact as any timestep where the closest heavy atoms are less than 5 Å apart. While the vast majority of contacts are under 4 Å, this definition includes the many intermittent increases of separation to over 4 Å during an association event. (We also alternatively defined a contact as any timestep where the RB center-of-mass was within 8 Å of the center of any

atom on the polymer, since 8 Å is roughly the molecular radius of the longest axis of RB; this produced extremely similar results.) To consider the influence of PBC, polyelectrolytes in the image cells were also included for analysis. Using the minimum-image convention, we computed the number of contacts, the total contact time, and the average duration of contact.

3. Results and Discussion

3.1. Polyelectrolyte Chain Dimensions

We begin by briefly presenting details of the simulated polyelectrolytes to verify that the simulations approximate what is known experimentally and theoretically about PSS and PDDA in aqueous salt solutions. The most salient factor here is that both the PSS 30-mer and PDDA 15-mer are short, rod-like chains whose structure and diffusion are consistent with theory, previous simulations, and extrapolated experimental data. Figure 5 shows the results of a clustering analysis that clearly reveals the general shape of the polymers during the entirety of the simulations. (For each polymer, 1,000 snapshots from each of the three simulation runs were grouped and analyzed, with only the backbone carbon atoms included in the analysis. The cluster centers are colored from black to white according to the cluster size, i.e. the black traces show the most populated cluster.) Table 3 lists the relevant polymer dimensions calculated for both the long chain and trimer forms of PDDA and PSS from the simulations, where each value represents an average over the entirety of the three 1-μs runs.

In the Supplementary Information we present extended comparisons of the simulated polymers with relevant theory, simulations, and experiments. This includes discussions of the parameters in Table 3, as well as persistence length, contour length, characteristic ratios, and the radial distribution functions for the counterions and water (Figures S1 and S2). Given these very short, fully charged polyelectrolyte chains, it is not surprising our results for end-to-end distance (r_{rms}) and radius of gyration ($R_{g,rms}$) are quite consistent with previous studies. All studies, including our simulations, agree that these short chains in 0.1 M NaCl are not entirely rod-like, despite their fairly straight appearance in Figure 5. The ratio $<r^2>/<R_g^2>$ is expected to be 6 for a Gaussian chain (i.e. a random coil that obeys a Gaussian random walk model) and 12 for a rigid rod.[110,111] Table 3 indicates this ratio is 9.2 for PSS and 7.8 for PDDA, putting both in a regime that is neither coiled nor a rigid rod; this is reflected in the conformational sampling of Figure 5, where it is also evident that PDDA is less rod-like than PSS. The relatively high salt concentration helps in screening repulsive charges on both chains, which adds some flexibility to the backbone.

3.2. PE trimer diffusion in solution

Table 4 lists all the relevant raw and corrected diffusion coefficients from the simulations (see section 2.2 for details on the derivation of these values). The PE diffusion (first four rows of Table 4) is discussed at length in the Supplementary Information in relation to theory and previous studies. Here we briefly discuss the faster observed PDDA trimer diffusion compared to PSS trimer diffusion, given its relevance for the observed diffusion of RB in those solutions. The faster PDDA trimer diffusion is interesting, because while they have similar R_g values, the PDDA end-to-end distance is twice that of PSS (Table 3).

However, our simulations show that ~10% of the PSS trimer molecules are present at any given time as dimers, or even trimers, whereas virtually all the PDDA trimers are present as monomers. We attribute this to the fact that sodium counterions are much more likely to be condensed on PSS compared to the sodium counterions of PDDA (Figure S1). Net neutral PSS trimers will aggregate more readily than oppositely charged PDDA trimers, leading to a lower average PSS trimer diffusion. Whether this is the sole cause of the slower PSS trimer diffusion is unclear; it may be that counterion condensation itself slows diffusion, also.

3.3. RB diffusion in solution

3.3.1. RB diffusion in polymer-free solutions—As a further test of our simulation methods, we calculated the diffusion of RB in neat water and NaCl solution, using the same size box as for the other simulations with polyelectrolytes. Given the relative simplicity of the system, 300 ns simulations were sufficient to extract diffusion coefficients with acceptable errors. The D_0 values (Table 4) show excellent correspondence to experiment, especially when the slightly higher 300 K temperature is accounted for compared to experiment. Gendron et al. report in a careful NMR diffusion study of four rhodamine dyes $D = 4.2 \pm 0.3 \times 10^{-6}$ cm^2/s for RB in < 0.1 M salt solutions.[113] This value for R6G was independently verified with FCS by Wang et al.[114] (As Gendron et al. discuss, this is higher than previously used values of 2.5–3.0 × 10^{-6} cm^2/s, e.g. in ref. 90.) These studies were both done at 22.5°C; adjusting the temperature and viscosity for 300 K with the Stokes-Einstein translational diffusion equation

$$D = \frac{kT}{6\pi\eta R_H} \tag{4}$$

where R_H is the hydrodynamic radius yields $D = 4.7 \times 10^{-6}$ cm^2/s, exactly the result of our simulations. Moreover, according to published data,[115] the NaCl solutions of 0.05 M and 0.1 M have similar enough viscosities so that D would only be changed in the third significant figure. (The slightly larger D_0 value for our 0.1 M NaCl simulation is not significantly different given the uncertainty estimates.)

3.3.2. RB diffusion in polyelectrolyte solutions—Having determined that the simulated polyelectrolytes and RB are individually behaving according to experiment, we turn to the crux of this study: the influence of polyelectrolytes on RB diffusion in solution. The most obvious effect, highlighted in Figure 6, is a slowdown in RB diffusion for all four polyelectrolyte situations, as expected. Furthermore, there is a clear difference between RB diffusion in PDDA and in PSS. RB diffusion in the presence of the PSS 30-mer is significantly lower than free RB diffusion, with $D_0 = 4.2 \times 10^{-6}$ cm^2/s compared to 4.7 × 10^{-6} cm^2/s for free RB (Table 4). In the presence of the two PDDA 15-mers, however, RB diffusion is substantially slower (2.2 × 10^{-6} cm^2/s). Some of this may be explained by the fact that despite $c_{PDDA} < c_{PSS}$ (Table S4, 13.2 g/L of PDDA vs. 19.2 g/L for PSS), the total contour length of two PDDA 15-mers (82 Å for one 15-mer) is more than twice as long as one PSS 30-mer (76 Å). More interesting is the effect on RB diffusion of the trimer solutions. Ten PSS trimers are seen to significantly slow down RB diffusion compared to the one 30-mer. However, ten PDDA trimers *increase* RB diffusion relative to the two PDDA 15-mers, and the D_0 value is actually greater than for the ten PSS trimers. As seen below,

these diffusion results for RB in the presence of various polyelectrolytes are best explained in terms of RB/PE association.

3.3.3. Considerations of volume exclusion and crowder size—A polymer solution has a higher bulk viscosity than pure water, and therefore according to the Stokes-Einstein equation (eq 4) the RB diffusion should slow down. However, as detailed in the Supplementary Information, the bulk viscosities of the PE solutions do not fully explain the observed RB diffusion data. RB is slowed more than predicted, meaning it experiences a microviscosity which is larger than the bulk viscosity. Moreover, the trimer vs. long-chain results are not explained by considerations of bulk viscosity.

A molecular understanding of decreasing diffusion with increasing bulk viscosity relies on the concept of a *crowder*, which is any solute that limits the ability of a diffuser to access bulk water through volume exclusion. (Closely related are *viscogens* which refer to any solute that increases the viscosity of the solution.) Decades of data and theory regarding tracer and probe diffusion in polymer solutions has led to several equations relating D to crowder concentration. In the Supplementary Information we explore several models and demonstrate that none are sufficient to fully explain either the magnitudes or trimer/long-chain variations of Figure 6. We want to highlight here the relevance to our work of the Zhang et al. study cited in Table S5.[34] This is a FCS experiment where the diffusion of various neutral and charged probes were measured in 20 kDa polyethylene glycol (PEG) and three types of dextrans: anionic, cationic, and neutral. Their main finding was that while in neutral PEG all probes obeyed unique exponential scaling relations, a charged probe had much reduced diffusion and a non-exponential dependence on concentration in the oppositely charged dextran. These charged probes, however, did follow an exponential model in the presence of neutral and like-charged dextran, suggesting that the zwitterionic RB of our study, which has relatively short-lived associations with the various PE crowders, is behaving somewhere between what would be expected for a neutral dye and a charged dye. Using their results for the positively charged rhodamine 6G (R6G) in neutral PEG and comparing to our PE concentrations, we would predict D_0 to be 3.5×10^{-6} cm^2/s for PSS and 3.8×10^{-6} cm^2/s for PDDA. This shows that while crowder effects alone can explain a decrease of RB diffusion very close to the values we see for the trimers, clearly other factors must be at play to fully explain our long-chain data.

The only other possible effect to consider besides RB/PE association is the relative sizes of the crowder molecules. Vilaseca et al. have shown through Monte Carlo simulations that obstacle (crowder) size also matters a great deal at a given fraction of excluded volume.[116,117] They demonstrate that in addition to excluded volume, the spatial distribution pattern of the crowder also affects D for a probe. As first glance, this seems to be precisely the effect we have observed here, where the presence of PSS or PDDA as either long chains or trimers has different effects on RB diffusion, even though the overall excluded volume is roughly the same. Vilaseca et al. show that for non-attractive mobile obstacles, smaller-sized obstacles inhibit diffusion more than larger obstacles for the same fraction of excluded volume, which is what we have observed in our PSS simulations. However, the magnitude of the obstacle effect in general, small or large, is far greater in our simulations than in Vilaseca et al., who show for excluded volumes less than 5%, which is the concentration

regime of our simulations, D/D_{neat} is still ≥ 0.95 for all obstacle sizes, including those that are the same size as the diffusion probe (such as our trimers compared to RB), while D/D_{neat} for our systems ranges from 0.46 to 0.89 (Table S4). Additionally, PDDA reverses the trend observed in obstacle size, in that our PDDA trimers promote RB diffusion more than the larger 15-mers. Both of these results, the larger magnitude of diffusion slow-down in our simulations and the opposite effects of obstacle size on RB diffusion between PSS and PDDA, indicate that attractive forces must be significantly at play between RB and the polyelectrolytes.

3.3.4. Analysis of tracer/crowder attractions—We have found that the variable data of Figure 6 is mostly a reflection of the variable nature of the RB/PE associations in each system. Table 5 presents results of analyzing the RB/PE contacts in all our simulations. ('Contact' is taken to be any timestep where the RB/PE distance is < 5 Å, and an 'association event' is taken to be a continuous contact that lasts longer than 0.5 ns.) Several important trends emerge from this contact analysis. First, PDDA has significantly longer average association times with RB than PSS, and also longer cumulative association times. This explains the lower RB D_0 values with long-chain PDDA vs. PSS. Second, both PSS and PDDA trimers have more RB contacts than the corresponding long chain, and also a larger number of association events > 0.5 ns. This is attributed partially to a crowder-size effect since the trimers are more spread out through the simulation box than the long-chain polymers, making contact with RB more likely. Also at play, though, is the shorter average association time with trimers, freeing RB to make more contacts. For PSS, however, the 2-fold longer average RB association with the 30-mers does not completely account for the 5-fold decrease in association events compared to the trimers. As a result, even though the average RB contact duration with PSS trimers is shorter than with the 30-mer, the cumulative contact duration for trimers is much longer than the PSS long chain. Conversely, the PDDA trimer cumulative RB contact time is virtually the same as for the PDDA long chain. This is because the 2.4-fold longer average association time with the PDDA 15-mers is balanced by the 2.4 decrease in associations events compared to the trimers. The stronger attraction of RB to PDDA and longer association times, together with the faster diffusion of PDDA trimers relative to PSS trimers, override the crowder-size contact effect observed in the PSS systems.

Figure 7 helps illuminate the average values of the contact data by plotting the lengths of individual associations for each of the four systems. Each histogram collects contact events from all three triplicate runs for each system. For the PSS 30-mer and PDDA 15-mers, there are clearly more longer events than for their respective trimers, indicating the long chains are clearly more adept at holding onto RB for long times. This is also observed in the much larger number of events under 20 ns for the trimers compared to the long chains. Also clear is the greater attraction of RB for PDDA than for PSS; both the PDDA long chains and trimers have more long associations than the corresponding PSS. Finally, the most likely type of contact in each system are those under 1 ns; they are 10–100 times more prevalent than the 1–2 ns events. The inset on each of the charts is a histogram of contacts under 2 ns with a narrower bin width of 100 ps rather than 1 ns. The similar-looking insets indicate that the vast majority of the contact durations in the 1 ns bin are in a very short

100 ps window and are due to non-associative collisions. As discussed in more detail in the Supplementary Information, there is a clear distinction to be made between very short, non-associative contacts that are diffusion-limited in duration and much longer, associative contacts, the latter of which are primarily responsible for the observed variations in the RB D_0 values.

3.3.5. Two-component diffusion model—In comparing the PSS and PDDA diffusion results overall, the striking difference is that while RB diffusion in the long-chain PDDA solution is much slower than in the long-chain PSS, the exact opposite is true in the case of the trimers. This is primarily due to the fast diffusion of the PDDA trimers themselves relative to the PSS trimers (Table 4), so when RB associates with the PDDA trimer, the complex diffuses faster than when RB associates with the PSS trimers.

The RB diffusion in the various polyelectrolyte systems is well-explained on these sub-1 μs timescales by invoking a simple two-component diffusion model, similar to many other studies,[35,45,60,65,88,89]

$$D_{eff} = f_{free} D_{free} + f_{bound} D_{bound} \quad (5)$$

where f is the fraction of time RB spends free and bound. A two-state model is also justified by the potential of mean force calculations (Figure S5) which show one distinct attractive well for RB around 3.5 Å for both long-chain PEs, and a small barrier near 5 Å. To facilitate this analysis, we extracted D_{bound} and D_{free} from an alternate set of MSD curves generated separately from RB diffusion while in contact with the PE and for free RB not in contact with a PE. A 1 μs run was separated into two groups of sub-runs: those periods where RB was in contact with a PE throughout the sub-run and those where RB was not in contact throughout the sub-run. Bound and free MSDs were then created from the two groups of sub-runs. Figure 8 shows these split MSD plots from one run of each of the four systems, along with the linear fit. The fraction of time RB is bound to PE in each system, f_{bound}, is assumed to be the total association time (time spent in sub-runs longer than 0.5 ns) divided by 1 μs, and $f_{\text{free}} = 1 - f_{\text{bound}}$. This assumes only associations longer than 0.5 ns have a significant effect on slowing RB diffusion. Results of this analysis are given in Table 6. As shown by the ratios $D_{0,\text{RB}}/D_{\text{eff}}$, which are all close to 1, the two-component model reproduces quite well the measured $D_{0,\text{RB}}$ values from Table 4. Only for the PDDA 15-mer system is the match not within the error. As discussed in the next section, this system produces the most anomalous RB diffusion at early times, which could explain this poorer fit of the simple two-state model which assumes normal (Fickian) diffusion. Given the relatively poor statistics obtained for the MSDs of free RB, we also calculated D_{eff}* assuming unbound RB diffuses with a value corresponding to the value measured in PE-free solutions (4.7×10^{-7} cm^2/sec).

There are several additional items that warrant brief discussion from these two-component diffusion results. First, D_{bound} for RB associating with the long chain polymers is *larger* than the D_0 values for the bare PE (Table 4). If the RB were covalently attached to either the PSS 30-mer or the PDDA 15-mer, the D_{bound} value would be expected to be lower than the bare PE. The larger D_{bound} values must reflect the loose association of RB with the PE, where

RB occasionally moves more quickly while still being within contact distance of the PE. As discussed more below, we find the RB samples quite a wide range of the PE backbone while staying in contact. The other alternative, that the presence of RB causes the PE chain to coil further and adopt a smaller R_G, was not found to be significant. Second, it is interesting that D_{free} values are all uniformly lower than the simulated $D_{0,RB}$ in PE-free solutions (Table 4), which likely reflects crowding effects due to the PE, though necessarily at non-contact distances.

Lastly, the two-state model is a simplification that highlights the dominant dynamics in these systems. However, there are a few factors that are left out that may subtly affect diffusion. One factor is assuming all contacts under 0.5 ns involve free RB diffusion; if those contacts are slower, that would lower D_{eff}. Another factor is the difference in dynamics of water surrounding the PEs (so-called 'biological water'[118–121]) from bulk water. This difference could mean diffusion close to PEs, but not within 5 Å, could be different than the measured D_{free}.

3.3.6. Anomalous versus normal diffusion—Further insight into the simulated RB diffusion in PE solutions is gained by characterizing the early-time diffusion as being either normal or anomalous. The plots of Figure 9 are the accepted manner of determining this characterization. For normal diffusion MSD increases linearly with time (eq 2), so a plot of $MSD(t)/t$ vs. t will yield a horizontal line at $6D$. Anomalous diffusion describes the situation where, over a given time window, MSD does not increase linearly with time. It is described by the anomalous diffusion exponent, α, where MSD ~ t^{α}. When $\alpha < 1$ the process is 'sub-diffusive' since MSD is increasing slower than in normal diffusion. Any deviation of the MSD/t vs. t from a horizontal plot indicates anomalous diffusion. Typically, what is seen for anomalous diffusion is sub-diffusive behavior, characterized by an initial steady decrease of MSD/t until a cross-over time, t_c, when the plot levels off and the diffusion becomes normal at longer timescales. With all manner of studies (theoretical, simulated, experimental) the key parameter is the timescale over which diffusion is being measured. Obstacles that produce anomalous diffusion on a shorter timescale are simply part of a macroscopic viscosity that yields normal diffusion on a longer timescale. This distinction, though, is not just one of investigative method; many natural and physical processes have inherent time limits during which diffusion occurs, meaning these systems often never reach a normal diffusive regime. Characterizing the anomalous diffusion thus becomes vitally important to fully understand such systems.

The top plot in Figure 9 of RB diffusing in 100 mM NaCl solution is typical for the RB-only simulations. After a subtle rise between 10 and 100 ps (reflecting early-time increasing 'ballistic' diffusion), MSD/t becomes horizontal in all the trajectories out to nearly 10 ns. This is entirely as expected—normal diffusion in the absence of molecular crowders. The root-mean-square distance ($MSD^{1/2}$) diffused during this time is more than five RB diameters (long-axis diameter is ~1.6 nm). (The truncated plot is due to the RB/water simulations only being 300 ns long.)

For RB diffusion in the PSS solutions, we see different behavior between the 30-mer and the trimers. The 30-mer is similar to water—after a brief initial rise, by 100 ps MSD/t is flat

indicating normal diffusion. However, the trimer solution indicates anomalous diffusion to at least 5 ns when it seems to become normal, though the statistics become significantly worse beyond 10 ns for all the simulations. We might assign a lower limit of the t_c as 5 ns. The slope of MSD/t in the anomalous region on a log-log plot is equal to $\alpha - 1$. This gives $\alpha \approx 0.97$ for the PSS trimers, with a volume fraction of 2.5% (Table S4). The fact that the PSS 30-mer yields normal diffusion with $\alpha = 1$ cannot be attributed to its only slightly smaller volume fraction of 2.1% (Table S4), as other studies indicate a near-linear decrease of α with increasing volume fraction of crowder.

The anomalous diffusion in PSS trimers is interesting, because previous studies have indicated small, mobile crowders are more apt to lead to normal tracer diffusion than bigger, slower crowders at the same volume-percent concentration.[60,116,122,123] This is because the diffusing tracer takes less time to 'sense' the overall spatial distribution of crowders in its environment when they are small and well-distributed. We attribute the unusual PSS behavior to the attractive nature of the RB/PSS interactions. The RB has a much fuller distribution of contact durations under 10 ns to explore in the trimer solution than in the 30-mer (Figure 7). There are just a few long duration contacts in the 30-mer solution, with much fewer shorter term contacts. Evidently this disparity in the breadth of their contact distributions explains the length of time it takes for normal diffusion to set in. The crossover time, t_c, for the trimer solution is nearly two orders of magnitude from the onset of anomalous behavior, which is consistent with previous studies.

Figure 9 also indicates anomalous RB diffusion in the PDDA solutions. In this case, however, the longer chain system also shows anomalous diffusion, in contrast to the clear results of PSS showing normal diffusion in the long-chain system. Additionally, its α value (~0.90) is significantly smaller than the PDDA trimers (~0.99), again reversing the trend from PSS. We explain these results by first comparing with PSS. Both PDDA systems have far higher total contact times than either PSS system (Table 5); the PDDA 15-mers also have many more long duration contacts than the PSS 30-mer. Even more than in the case of the PSS trimers, this fuller distribution of contact durations induces anomalous diffusion. The PDDA trimers, on the other hand, only display slightly anomalous diffusion ($\alpha \approx 0.99$), as opposed to the clearly anomalous PSS trimers ($\alpha \approx 0.97$). This is also surprising, given the stronger RB attractions and longer average contact time compared to PSS. It must be that the faster diffusion of PDDA trimers vs. PSS trimers is a major contributor to minimizing the anomalous behavior in PDDA, e.g. Vilaseca et al. showed that increased mobility of crowders increases α, albeit in a non-associative system.[116] Lastly, we must compare the PDDA 15-mer and trimer results with each other. This is easier to explain, as the Vilaseca et al. study clearly shows that smaller mobile obstacles lead to less anomalous behavior than larger, less mobile obstacles. This is entirely related to their relative mobility, as the opposite trend was observed when the crowders were immobilized. The faster trimers enable the diffusing tracer to sample the overall average environment more quickly than with the slower 15-mers.

More detailed explorations of the observed anomalous diffusion are beyond the scope of this paper, e.g. assessing the nature of any ergodicity breaking[65] and characterizing the shapes of the van Hove particle distribution functions and their evolution in time. Given the general

success of a two-state model in explaining the trends in RB D values obtained from fits to the MSDs (Table 6), the close relation of this study to previous studies that employ a two-state model,[35,45] and the relatively small values of α, the assumption that RB undergoes normal (Fickian) diffusion characterized by a single D value during our 1 μs simulation is justified. Of course, this assumption is most tentative for the PDDA 15-mer system, but the general linearity of the MSDs between 2 and 20 ns for even this system suggests that on the time and length scales of this simulation it is reasonable. The weaker nature of PE/zwitterion binding and its faster on/off times allows both diffusion states to be sampled enough during 1 μs for normal diffusion to set in, whereas the stronger binding of a fully charged dye to a PE can lead to anomalous diffusion on much longer time scales, such as those interrogated by FCS.

3.4. Molecular-level analysis of RB/PE contacts

3.4.1. Atomic contact partners—Taking advantage of the fully atomistic simulations, we have analyzed the nature of the RB/PE associations at the molecular level. We were interested in further characterizing the contacts and elucidating why the RB/PDDA associations are longer-lasting than the RB/PSS associations. We first determined for all the simulation runs which RB heavy atom was closest to which PE heavy atom for every timestep. Several key results from this analysis are given in Table 7 and highlighted below.

For nearly 80% of the association time, the closest atoms of RB to PDDA (either the 15-mer or trimer) are typically the oxygen atoms, which are usually closest to one of the non-backbone carbon atoms of PDDA (and its partially positive hydrogen atom). The phenyl group on RB is typically rotated normal to the plane of the three-membered xanthenyl ring system, allowing the oxygen atom in the xanthenyl to also interact with the same atoms as the carboxylate oxygens. These three oxygens, together with the attendant carboxylate carbon, carry a total charge of −0.34. Six carbon atoms and their hydrogens accounted for 97% of the PDDA contact. There is a small preference for the ammonium methyls (C4 and C5, Figure 1) over the other two nitrogen-bound carbons and the two methylene carbons of the backbone chain. The two tertiary carbons are closest only 3% of the time, perhaps owing to their and their hydrogen's slightly smaller partial charges relative to their neighboring carbons.

On the other hand, the oxygens of the negatively charged sulfonate group of the PSS 30-mer only accounted for 29% of the closest atomic contacts with RB during association, and only 17% for the PSS trimers. One of the RB terminal methyls of the four nitrogen-bound ethyl groups is closest to the sulfonate 35% of the time, but many other RB carbons also spend time as the closest heavy atom to the sulfonate oxygens. The sulfonate group of PSS carries a net charge in this simulation of −0.36 (Table S1), which is nearly identical to the oxygen/carbon grouping in RB. Given that the RB hydrogens have a typical charge of ~ +0.15, like the PDDA hydrogens, it is a bit surprising that the sulfonate interactions with RB are so much less prevalent than the RB oxygen interactions with PDDA. Besides the obvious factor that each PDDA repeat unit has a net positive charge, though it is diffusely spread out, another factor increasing PDDA association times is likely the location of the RB oxygens. When a PDDA carbon is within contact range of the RB oxygens, the rest of the polymer is

necessarily in close contact with the RB as well, leading to additional van der Waal's-type attractions. The PSS oxygens, on the other hand, are far removed from the backbone and their interaction with RB does not necessarily engage the rest of the RB molecule. A further explanation of the more limited PSS sulfonate group interaction with RB could involve the counterions. As Figure S1 indicates, Na^+ is held on average much more closely to PSS than Cl^- is held to PDDA. Further analysis of any counterion effect is beyond the scope of this paper, but perhaps the close presence of Na^+ to the localized negative charge of the sulfonate group inhibits close association with RB, while the chloride anion has no localized home with PDDA and does not particularly hinder PDDA interaction with the RB carboxylate group.

3.4.2. Motion of RB along PE chain—The last major question to explore involves ascertaining how much of the polymer chain is involved in an association event. Is the RB basically stuck to one repeat unit of the polymer for the duration of an event, or does the RB move along the chain? To answer this, we chose a particular RB atom that is frequently closest to the PE and tracked how many PE repeat unit segments that atom contacted during a single association event. (For PSS we used the carbon in the 5 position of the phenyl ring, opposite the carboxylate group [C12 in Table S3 and Figure 1], and for PDDA one of the RB carboxylate oxygens.) While this atom will not always be the closest to the PE during an association event, it is the closest often enough to track the range of RB travel along the PE chain.

Figure 10 provides a visualization of the progression of two typical association events. The black left trace plots the RB motion back and forth along a PDDA 15-mer. The simulation time increases up the y-axis, while polymer repeat units have been numbered along the x-axis, with 1 corresponding to one end of the chain. This event from run 1 with the PDDA 15-mers lasts 10,609 timesteps. The RB oxygen switches quite often which PE segment it is closest to; particularly at the end of the run, the RB rattles back and forth between segments 6 and 7. This is due to the oxygen being between two ammonium methyl groups of adjacent PDDA segments. The gray trace at right plots RB moving along a PSS 30-mer (run 1). This plot shows some bigger jumps and a lower density of points since the RB atom we were tracking was the closest atom only a minority of the time. Both these graphs depict well the stochastic nature of the association event, but also the durability of the association between a zwitterion and polyelectrolyte of either charge.

Table 8 shows the cumulative results of this detailed analysis of association events, with the data binned into three groups based on the duration of the association (we ignored short-lived contacts less than 5 timesteps). Perhaps the most striking result is given in the third row of each entry, which shows the average duration of a single event in each bin (obtained by dividing the cumulative total association time in each bin category for the three runs divided by the total number of events in that bin). There is essentially no difference in the average event times for PDDA and PSS; in fact, for the longest associations, PSS has a slightly longer average binding time (36.1 vs. 32.9 ns). The fourth row for each entry, <# PE segments>, gives the average number of unique polymer segments involved in a single event. The shortest duration events typically involved only one PE segment, while the longest events involved an average of six PE segments for the long chains (and of course only

three segments are available with the trimers). These two rows (3rd and 4th) are remarkably similar quantitatively in all PE situations, which is surprising given the overall much longer cumulative contact time RB makes with PDDA compared to PSS (Table 5).

The final two rows in each data section of Table 8 describe a more detailed examination of the RB atom switching to a different PE segment. A ‘switch’ is counted when the RB is not simply rattling between two adjacent PE segments, but is truly making a translational motion along the PE chain. This excludes, for example, the many switches RB makes between PDDA segments 6 and 7 at the end of the event in Figure 10. What is found in each system is that the time spent between PE switches decreases as the event duration increases. This mostly reflects the fact that short events (0.05– 0.5 ns) predominantly have interactions with only one PE segment. As the association lengthens, more switches are possible. For PSS, the time per switch is fairly constant for the medium and long-term durations, while for PDDA there is a continued decrease in switch time as the durations lengthen (e.g. 0.255 ns for 15-mer events >5 ns compared to 0.663 ns for medium-length events). The PDDA switch time is also significantly less than the PSS switch time for longer events (0.255 vs. 1.11 ns for the long chains).

This faster segment switching time for RB with PDDA may actually be what increases the RB/PDDA contact time relative to PSS rather than inherently stronger molecular associations. Both Table 7 and Table 8 indicate the average nature of the long-term RB association events are very similar between PDDA and PSS—PDDA just has more of them. Perhaps the higher rate of switching reflects PDDA conformations that are more conducive than PSS to maintaining contact with RB as fluctuations cause it to translate and leave a particular contact spot. With PSS, a typical fluctuation might end the association event, whereas PDDA can more readily shift the RB to a new segment while maintaining contact. This may be linked to the larger overall flexibility of PDDA compared to PSS depicted in Figure 5.

Finally, as mentioned above, the motion of RB along the PE chain likely explains why D_{bound} for RB is greater than the corresponding PE D_0 value. For example, the PDDA 15-mer has $D_0 = 1.59 \times 10^{-6}$ cm^2/s (Table 4), while for RB $D_{bound} = 1.72 \times 10^{-6}$ cm^2/s (Table 6). On average, the additional RB diffusion along the PE chain will be normal to the net PE diffusion vector and leads to a longer MSD for RB over the same time. Using the average association duration of 32.9 ns for PDDA-15 and an average of 5.9 segments traversed by RB, together with a 5.5 Å monomer length for PDDA, a D_{bound} value of 1.8×10^{-6} cm^2/s is calculated, roughly in line with the simulations.

4. Conclusions

Fully atomistic MD simulations of zwitterionic rhodamine B in various polyelectrolyte solutions have provided insight into a number of important factors governing small molecule diffusion in crowded systems, including crowder identity, crowder size, and the molecular details of probe/crowder attractive interactions. This study demonstrates that a thorough analysis of the nature and interplay of all these important factors is required to fully understand the surprisingly complex probe diffusion dynamics, even in relatively dilute

systems. The two most obvious results from these simulations is a clear difference between the trimer and long-chain results for a single PE type, and the longer average RB binding time with PDDA compared to PSS. Clearly the size of the crowder plays a critical role in the measured RB dynamics, since each system has identical monomer concentrations and nearly identical volume percent of polymer. Furthermore, the RB diffusion in all the systems exhibits a positive deviation from Stokes-Einstein behavior, meaning RB experiences a microviscosity larger than the bulk viscosity and diffuses slower than expected.

The dominant feature of the RB/PE systems studied here, however, is the attractive interaction between RB and the polyelectrolyte, whether in its trimer or long-chain form. This result is some-what surprising, given that the RB zwitterion is overall charge neutral and therefore was not necessarily expected to form strong complexes with the PEs. Clearly the various other intermolecular forces, including the localized negative charge on the RB carboxylate group, are sufficient to produce persistent associations. A two-state model, where the measured RB diffusion is split between free diffusion and diffusion of a bound RB/PE complex, ultimately was needed to reproduce the important trends seen in the data. Specifically, the two-state model fits the slower RB diffusion in both PSS and PDDA long-chain solutions remarkably well. More impressively, it also matches the observed divergence of the trimer results. The PDDA trimers lead to faster RB diffusion than in the long-chain PDDA 15-mer solution, while the PSS trimers further decrease the RB diffusion relative to the long-chain PSS 30-mers. This difference is tied to the faster diffusion of PDDA trimers compared to the PSS trimers, which leads to faster RB/PDDA complexes.

While in general the wider dispersal of the smaller trimer should make RB contact more frequent than with a comparable volume of longer chain polymer, the longer average RB/PDDA association largely negates the crowder size effect that is observed with PSS. Because the average RB/PDDA contact time is so long, RB associates with the 15-mer as much as with the trimers. RB is not held as long to PSS, so there is a clear increase in contact time in the PSS trimer solution compared to the 30-mer. This key difference, along with the faster PDDA trimer diffusion compared to PSS trimers, fully explains the observed D_0 data. Why the PDDA/RB association is longer than PSS/RB has not been fully clarified. There are only two major differences we have uncovered, and that is the counterion condensation and the PE segment switching time. Determining the impacts on RB association of both the larger PDDA flexibility and the greater Na^+ condensation for PSS is a subject for further investigation.

The crowder size effect also manifests itself in the anomalous diffusion observed at early times in three of the four systems. This effect is not purely geometric, however, due to the RB/PE association. The relative strength of the associations determines what effect the size of the crowder has on the short-time diffusion. Stronger associations lead to more anomalous diffusion at short times, though this effect can be counter-balanced, as in the case of PDDA, with fast diffusion of the associative complex.

Finally, this work sheds light on small molecule diffusion in other dilute and semi-dilute polyelectrolyte systems. The observation that a zwitterion can form a short-lived complex with both polyanions and polycations that is not due to be being trapped or entangled by

a long chain is new and surprising. Whether these associations are due to RB being a zwitterion with a localized negative charge, or is a general feature of any neutral organic probe molecule, will be further studied. We plan to simulate the diffusion of both fully charged and non-zwitterionic neutral rhodamine analogues in similar PE solutions in an attempt to further disentangle the effects of attraction vs. crowding on small molecule transport in crowded environments. This study also suggests that counterion identity and level of condensation may have an indirect but important role on small molecule diffusion in PE solutions, primarily through its influence on PE/PE and PE/probe association.

Supplementary Material

Refer to Web version on PubMed Central for supplementary material.

Acknowledgments:

Funding was partially provided by the National Institutes of Health Grant R35 GM126948 (M.F.). P.W. thanks the High Performance Computing group at Wheaton College, specifically Neile Havens and Harvard Townsend, and funding from the Wheaton College Alumni Association and the Provost's Office. He also thanks early students on the project, including Drew Golz, Gabriel Cheeley, Drake Boyer, Tim Sedlacek, Ali McMillan, and Katie Whiteside.

References

(1). Schanze KS; Shelton AH Functional Polyelectrolytes. Langmuir 2009, 25 (24), 13698–13702. [PubMed: 20560548]

(2). Decher G; Schlenoff JT Multilayer Thin Films-Sequential Assembly of Nanocomposite Materials, 2nd ed.; Wiley-VCH: Weinheim, 2012.

(3). Decher G Fuzzy Nanoassemblies: Toward Layered Polymeric Multicomposites. Science 1997, 277, 1232–1237.

(4). Ariga K; Hill JP; Ji Q Layer-by-Layer Assembly as a Versatile Bottom-up Nanofabrication Technique for Exploratory Research and Realistic Application. Phys. Chem. Chem. Phys. 2007, 9, 2319–2340. [PubMed: 17492095]

(5). Jiang C; Saha A; Young CC; Hashim DP; Ramirez CE; Ajayan PM; Pasquali M; Marti AA Macroscopic Nanotube Fibers Spun from Single-Walled Carbon Nanotube Polyelectrolytes. ACS Nano 2014, 8 (9), 9107–9112. [PubMed: 25162378]

(6). Chung AJ; Rubner MF Methods of Loading and Releasing Low Molecular Weight Cationic Molecules in Weak Polyelectrolyte Multilayer Films. Langmuir 2002, 18 (4), 1176–1183.

(7). Alkekhia D; Hammond PT; Shukla A Layer-by-Layer Biomaterials for Drug Delivery. Annu. Rev. Biomed. Eng. 2020, 22.

(8). Anandhakumar S; Gokul P; Raichur AM Stimuli-Responsive Weak Polyelectrolyte Multilayer Films: A Thin Film Platform for Self Triggered Multi-Drug Delivery. Mater. Sci. Eng. C 2016, 58, 622–628.

(9). Shamoun RF; Reisch A; Schlenoff JB Extruded Saloplastic Polyelectrolyte Complexes. Adv. Funct. Mater. 2012, 22 (9), 1923–1931.

(10). Yang M; Digby ZA; Schlenoff JB Precision Doping of Polyelectrolyte Complexes: Insight on the Role of Ions. Macromolecules 2020, 53 (13), 5465–5474.

(11). Sciortino F; Mir SH; Pakdel A; Oruganti A; Abe H; Witecka A; Shri DNA; Rydzek G; Ariga K Saloplastics as Multiresponsive Ion Exchange Reservoirs and Catalyst Supports. J. Mater. Chem. A 2020, 8 (34), 17713–17724.

(12). Mecerreyes D Polymeric Ionic Liquids: Broadening the Properties and Applications of Polyelectrolytes. Prog. Polym. Sci. 2011, 36 (12), 1629–1648.

(13). Forsyth M; Porcarelli L; Wang X; Goujon N; Mecerreyes D Innovative Electrolytes Based on Ionic Liquids and Polymers for Next-Generation Solid-State Batteries. Acc. Chem. Res. 2019, 52 (3), 686–694. [PubMed: 30801170]

(14). Oh S; Nikolaev A; Tagami K; Tran T; Lee D; Mukherjee S; Segalman RA; Han S; Read de Alaniz J; Chabinyc ML Redox-Active Polymeric Ionic Liquids with Pendant N-Substituted Phenothiazine. ACS Appl. Mater. Interfaces 2021, 13 (4), 5319–5326. [PubMed: 33480673]

(15). Thomas EM; Nguyen PH; Jones SD; Chabinyc ML; Segalman RA Electronic, Ionic, and Mixed Conduction in Polymeric Systems. Annu. Rev. Mater. Res. 2021, 51.

(16). Bradley DF; Wolf MK Aggregation of Dyes Bound to Polyanions. Proc. Natl. Acad. Sci. U. S. A. 1959, 45 (7), 944. [PubMed: 16590488]

(17). Thompson CJ; Cheng WP Chemically Modified Polyelectrolytes for Intestinal Protein and Peptide Delivery. In Peptide and Protein Delivery; Van Der Walle C, Ed.; Elsevier, 2011; pp 123–158.

(18). Wang K; Wei T; Li Y; He L; Lv Y; Chen L; Ahmad A; Xu Y; Shi Y Flocculation-to-Adsorption Transition of Novel Salt-Responsive Polyelectrolyte for Recycling of Highly Polluted Saline Textile Effluents. Chem. Eng. J. 2021, 413, 127410.

(19). Akboura RA; El Gaaydaa J; Titchoua FE; Khenifib A; Afangaa H; Farahic A; Yapd P-S; Fortee MBS; Hamdania M Adsorption of Anionic Dyes from Aqueous Solution Using Polyelectrolyte PDAD-PDADMAC-Modified-Montmorillonite Clay. Desalination Water Treat 2020, 208, 407–422.

(20). Huang S; Zhao M; Dawadi MB; Cai Y; Lapitsky Y; Modarelli DA; Zacharia NS Effect of Small Molecules on the Phase Behavior and Coacervation of Aqueous Solutions of Poly (Diallyldimethylammonium Chloride) and Poly (Sodium 4-Styrene Sulfonate). J. Colloid Interface Sci. 2018, 518, 216–224. [PubMed: 29459301]

(21). Inoue K; Aikawa S; Masaru S; Fukushima Y Colorimetric Chemosensor for Fe 2+ and Fe 3+ Based on a Ternary Mixture of an Anionic Dye, a Cationic Polyelectrolyte, and a Metal Chelator in Aqueous Solution. J. Incl. Phenom. Macrocycl. Chem. 2018, 91 (3), 171–177.

(22). Inoue K; Aikawa S; Sakamaki M; Fukushima Y Colorimetric Co2+ Sensor Based on an Anionic Pyridylazo Dye and a Cationic Polyelectrolyte in Aqueous Solution. Polym. Int. 2018, 67 (12), 1589–1594.

(23). Tanwar AS; Iyer PK Fluorescence “Turn-on” Indicator Displacement Assay-Based Sensing of Nitroexplosive 2, 4, 6-Trinitrophenol in Aqueous Media via a Polyelectrolyte and Dye Complex. ACS Omega 2017, 2 (8), 4424–4430. [PubMed: 31457734]

(24). Pronkin PG; Tatikolov AS Formation of J-Aggregates of an Anionic Oxacarbocyanine Dye upon Interaction with Proteins and Polyelectrolytes. J. Appl. Spectrosc. 2017, 84 (2), 217–224.

(25). Zhao M; Wang C; Jiang H; Dawadi MB; Vogt BD; Modarelli DA; Zacharia NS Polyelectrolyte–Micelle Coacervates: Intrapolymer-Dominant vs. Interpolymer-Dominant Association, Solute Uptake and Rheological Properties. Soft Matter 2019, 15 (14), 3043–3054. [PubMed: 30901008]

(26). Yethiraj A Liquid State Theory of Polyelectrolyte Solutions. J. Phys. Chem. B 2009, 113 (6), 1539–1551. [PubMed: 19035818]

(27). Dautzenberg H; Görnitz E; Jaeger W Synthesis and Characterization of Poly (Diallyldimethylammonium Chloride) in a Broad Range of Molecular Weight. Macromol. Chem. Phys. 1998, 199 (8), 1561–1571.

(28). Marcelo G; Tarazona MP; Saiz E Solution Properties of Poly (Diallyldimethylammonium Chloride)(PDDA). Polymer 2005, 46 (8), 2584–2594.

(29). Babaye Khorasani F; Poling-Skutvik R; Krishnamoorti R; Conrad JC Mobility of Nanoparticles in Semidilute Polyelectrolyte Solutions. Macromolecules 2014, 47 (15), 5328–5333.

(30). Slim AH; Poling-Skutvik R; Conrad JC Local Confinement Controls Diffusive Nanoparticle Dynamics in Semidilute Polyelectrolyte Solutions. Langmuir 2020, 36 (31), 9153–9159. [PubMed: 32678607]

(31). Phillies GD; Malone C; Ullmann K; Ullmann GS; Rollings J; Yu LP Probe Diffusion in Solutions of Long-Chain Polyelectrolytes. Macromolecules 1987, 20 (9), 2280–2289.

(32). Furukawa R; Arauz-Lara JL; Ware BR Self-Diffusion and Probe Diffusion in Dilute and Semidilute Aqueous Solutions of Dextran. Macromolecules 1991, 24 (2), 599–605.

(33). Bu Z; Russo PS Diffusion of Dextran in Aqueous (Hydroxypropyl)Cellulose. Macromolecules 1994, 27 (5), 1187–1194. 10.1021/ma00083a017.

(34). Zhang X; Hansing J; Netz RR; DeRouchey JE Particle Transport through Hydrogels Is Charge Asymmetric. Biophys. J. 2015, 108 (3), 530–539. 10.1016/j.bpj.2014.12.009. [PubMed: 25650921]

(35). Vagias A; Raccis R; Koynov K; Jonas U; Butt H-J; Fytas G; Košovan P; Lenz O; Holm C Complex Tracer Diffusion Dynamics in Polymer Solutions. Phys. Rev. Lett. 2013, 111 (8), 088301. 10.1103/PhysRevLett.111.088301. [PubMed: 24010481]

(36). Cherdhirankorn T; Best A; Koynov K; Peneva K; Muellen K; Fytas G Diffusion in Polymer Solutions Studied by Fluorescence Correlation Spectroscopy. J. Phys. Chem. B 2009, 113 (11), 3355–3359. 10.1021/jp809707y. [PubMed: 19228045]

(37). Dauty E; Verkman AS Molecular Crowding Reduces to a Similar Extent the Diffusion of Small Solutes and Macromolecules: Measurement by Fluorescence Correlation Spectroscopy. J. Mol. Recognit. 2004, 17 (5), 441–447. [PubMed: 15362103]

(38). Okur HI; Hladílková J; Rembert KB; Cho Y; Heyda J; Dzubiella J; Cremer PS; Jungwirth P Beyond the Hofmeister Series: Ion-Specific Effects on Proteins and Their Biological Functions. J. Phys. Chem. B 2017, 121 (9), 1997–2014. [PubMed: 28094985]

(39). Salomäki M; Tervasmäki P; Areva S; Kankare J The Hofmeister Anion Effect and the Growth of Polyelectrolyte Multilayers. Langmuir 2004, 20, 3679–3683. [PubMed: 15875399]

(40). Jaber JA; Schlenoff JB Counterions and Water in Polyelectrolyte Multilayers: A Tale of Two Polycations. Langmuir 2007, 23, 896–901. [PubMed: 17209649]

(41). Chremos A; Douglas JF Counter-Ion Distribution around Flexible Polyelectrolytes Having Different Molecular Architecture. Soft Matter 2016, 12 (11), 2932–2941. [PubMed: 26864861]

(42). Chremos A; Douglas JF Polyelectrolyte Association and Solvation. J. Chem. Phys. 2018, 149 (16), 163305. [PubMed: 30384680]

(43). Yu J; Jackson NE; Xu X; Morgenstern Y; Kaufman Y; Ruths M; De Pablo JJ; Tirrell M Multivalent Counterions Diminish the Lubricity of Polyelectrolyte Brushes. Science 2018, 360 (6396), 1434–1438. [PubMed: 29954973]

(44). Zheng K; Chen K; Ren W; Yang J; Zhao J Counterion Cloud Expansion of a Polyelectrolyte by Dilution. Macromolecules 2018, 51 (12), 4444–4450. 10.1021/acs.macromol.8b00075.

(45). Jia P; Yang Q; Gong Y; Zhao J Dynamic Exchange of Counterions of Polystyrene Sulfonate. J. Chem. Phys. 2012, 136 (8), 084904. 10.1063/1.3688082. [PubMed: 22380063]

(46). Xu G; Luo S; Yang Q; Yang J; Zhao J Single Chains of Strong Polyelectrolytes in Aqueous Solutions at Extreme Dilution: Conformation and Counterion Distribution. J. Chem. Phys. 2016, 145 (14), 144903. 10.1063/1.4964649. [PubMed: 27782532]

(47). Krishnamoorthy AN; Holm C; Smiatek J Specific Ion Effects for Polyelectrolytes in Aqueous and Non-Aqueous Media: The Importance of the Ion Solvation Behavior. Soft Matter 2018, 14 (30), 6243–6255. [PubMed: 30009285]

(48). Lyubartsev AP Molecular Simulations of DNA Counterion Distributions. Encycl. Nanosci. Nanotechnol. HS Nalwa Ed. Marcel Dekker N. Y. 2004, 2131–2143.

(49). Smiatek J Theoretical and Computational Insight into Solvent and Specific Ion Effects for Polyelectrolytes: The Importance of Local Molecular Interactions. Molecules 2020, 25 (7), 1661. [PubMed: 32260301]

(50). Rivas G; Minton AP Macromolecular Crowding in Vitro, in Vivo, and in Between. Trends Biochem. Sci. 2016, 41 (11), 970–981. [PubMed: 27669651]

(51). Khandai S; Jena SS Transition from Double to Single Diffusive Behavior with Increase in Polymer Concentration for Oppositely Charged Guest–Host Systems of Green Fluorescent Protein Diffusing inside Poly-l-Lysine Solutions. J. Colloid Interface Sci. 2017, 505, 196–205. [PubMed: 28578282]

(52). Nogueira TPO; Frota HO; Piazza F; Bordin JR Tracer Diffusion in Crowded Solutions of Sticky Polymers. Phys. Rev. E 2020, 102 (3), 032618. [PubMed: 33075900]

(53). Blanco PM; Garcés JL; Madurga S; Mas F Macromolecular Diffusion in Crowded Media beyond the Hard-Sphere Model. Soft Matter 2018, 14 (16), 3105–3114. [PubMed: 29620120]

(54). Moreno-Villoslada I; Jofré M; Miranda V; González R; Sotelo T; Hess S; Rivas BL PH Dependence of the Interaction between Rhodamine B and the Water-Soluble Poly (Sodium 4-Styrenesulfonate). J. Phys. Chem. B 2006, 110 (24), 11809–11812. [PubMed: 16800481]

(55). Dix JA; Verkman AS Crowding Effects on Diffusion in Solutions and Cells. Annu Rev Biophys 2008, 37, 247–263. [PubMed: 18573081]

(56). Phillies GD Optical Probe Diffusion in Polymer Solutions. ArXiv Prepr. ArXiv07053222 2007.

(57). Ernst D; Köhler J; Weiss M Probing the Type of Anomalous Diffusion with Single-Particle Tracking. Phys. Chem. Chem. Phys. 2014, 16 (17), 7686–7691. [PubMed: 24651929]

(58). Szymanski J; Weiss M Elucidating the Origin of Anomalous Diffusion in Crowded Fluids. Phys. Rev. Lett. 2009, 103 (3), 038102. [PubMed: 19659323]

(59). Thiel F; Flegel F; Sokolov IM Disentangling Sources of Anomalous Diffusion. Phys. Rev. Lett. 2013, 111 (1), 010601. [PubMed: 23862987]

(60). Geyer T Mixing Normal and Anomalous Diffusion. J. Chem. Phys. 2012, 137 (11), 115101. [PubMed: 22998287]

(61). Samanta N; Chakrabarti R Tracer Diffusion in a Sea of Polymers with Binding Zones: Mobile vs. Frozen Traps. Soft Matter 2016, 12 (41), 8554–8563. 10.1039/C6SM01943A. [PubMed: 27714359]

(62). Feig M; Sugita Y Variable Interactions between Protein Crowders and Biomolecular Solutes Are Important in Understanding Cellular Crowding. J. Phys. Chem. B 2012, 116 (1), 599–605. [PubMed: 22117862]

(63). Metzler R; Jeon J-H; Cherstvy AG; Barkai E Anomalous Diffusion Models and Their Properties: Non-Stationarity, Non-Ergodicity, and Ageing at the Centenary of Single Particle Tracking. Phys. Chem. Chem. Phys. 2014, 16 (44), 24128–24164. [PubMed: 25297814]

(64). Cherstvy AG; Thapa S; Wagner CE; Metzler R Non-Gaussian, Non-Ergodic, and Non-Fickian Diffusion of Tracers in Mucin Hydrogels. Soft Matter 2019, 15 (12), 2526–2551. [PubMed: 30734041]

(65). Grebenkov DS Time-Averaged Mean Square Displacement for Switching Diffusion. Phys. Rev. E 2019, 99 (3), 032133. [PubMed: 30999505]

(66). Foldes-Papp Z; Baumann G Fluorescence Molecule Counting for Single-Molecule Studies in Crowded Environment of Living Cells without and with Broken Ergodicity. Curr. Pharm. Biotechnol. 2011, 12 (5), 824–833. [PubMed: 21446904]

(67). Yu Y; Anthony SM; Bae SC; Granick S How Liposomes Diffuse in Concentrated Liposome Suspensions. J. Phys. Chem. B 2011, 115 (12), 2748–2753. [PubMed: 21384815]

(68). Saxton MJ Anomalous Diffusion Due to Obstacles: A Monte Carlo Study. Biophys. J. 1994, 66 (2), 394–401. 10.1016/S0006-3495(94)80789-1. [PubMed: 8161693]

(69). Saxton MJ Anomalous Diffusion Due to Binding: A Monte Carlo Study. Biophys. J. 1996, 70 (3), 1250–1262. [PubMed: 8785281]

(70). Vlahos L; Isliker H; Kominis Y; Hizanidis K Normal and Anomalous Diffusion: A Tutorial. ArXiv Prepr. ArXiv08050419 2008.

(71). Phillies GD Diffusion on a Molecular Scale as Observed Using PGSE NMR. Concepts Magn. Reson. Part A 2015, 44 (1), 1–15.

(72). Kumar P; Theeyancheri L; Chaki S; Chakrabarti R Transport of Probe Particles in a Polymer Network: Effects of Probe Size, Network Rigidity and Probe–Polymer Interaction. Soft Matter 2019, 15 (44), 8992–9002. [PubMed: 31681926]

(73). Magdziarz M; Weron A Anomalous Diffusion: Testing Ergodicity Breaking in Experimental Data. Phys. Rev. E 2011, 84 (5), 051138.

(74). Sorichetti V; Hugouvieux V; Kob W Dynamics of Nanoparticles in Polydisperse Polymer Networks: From Free Diffusion to Hopping. Macromolecules 2021.

(75). Cho HW; Kim H; Sung BJ; Kim JS Tracer Diffusion in Tightly-Meshed Homogeneous Polymer Networks: A Brownian Dynamics Simulation Study. Polymers 2020, 12 (9), 2067. [PubMed: 32932910]

(76). Dechant A; Lutz E; Kessler DA; Barkai E Scaling Green-Kubo Relation and Application to Three Aging Systems. Phys. Rev. X 2014, 4 (1), 011022.

(77). Sokolov IM Models of Anomalous Diffusion in Crowded Environments. Soft Matter 2012, 8 (35), 9043–9052.

(78). Lyulin SV; Vattulainen I; Gurtovenko AA Complexes Comprised of Charged Dendrimers, Linear Polyelectrolytes, and Counterions: Insight through Coarse-Grained Molecular Dynamics Simulations. Macromolecules 2008, 41 (13), 4961–4968. 10.1021/ma800736p.

(79). Carrillo J-MY; Dobrynin AV Polyelectrolytes in Salt Solutions: Molecular Dynamics Simulations. Macromolecules 2011, 44 (14), 5798–5816. 10.1021/ma2007943.

(80). Poghosyan AH; Arsenyan LH; Gharabekyan HH; Koetz J; Shahinyan AA Molecular Dynamics Study of Poly (Diallyldimethylammonium Chloride)(PDADMAC)/Sodium Dodecyl Sulfate (SDS)/Decanol/Water Systems. J. Phys. Chem. B 2009, 113 (5), 1303–1310. [PubMed: 19175342]

(81). Tucker AK; Stevens MJ Study of the Structure Dependent Behavior of Polyelectrolyte in Water. J. Chem. Phys. 2013, 139 (10), 104907. [PubMed: 24050365]

(82). Mafi A; Abbina S; Kalathottukaren MT; Morrissey JH; Haynes C; Kizhakkedathu JN; Pfaendtner J; Chou KC Design of Polyphosphate Inhibitors: A Molecular Dynamics Investigation on Polyethylene Glycol-Linked Cationic Binding Groups. Biomacromolecules 2018, 19 (4), 1358–1367. 10.1021/acs.biomac.8b00327. [PubMed: 29539260]

(83). Vishnyakov A; Neimark AV Specifics of Solvation of Sulfonated Polyelectrolytes in Water, Dimethylmethylphosphonate, and Their Mixture: A Molecular Simulation Study. J. Chem. Phys. 2008, 128 (16), 164902. 10.1063/1.2899327. [PubMed: 18447495]

(84). Qiao B; Cerdà JJ; Holm C Poly(Styrenesulfonate)−Poly(Diallyldimethylammonium) Mixtures: Toward the Understanding of Polyelectrolyte Complexes and Multilayers via Atomistic Simulations. Macromolecules 2010, 43 (18), 7828–7838. 10.1021/ma101091k.

(85). Qiao B; Cerdà JJ; Holm C Atomistic Study of Surface Effects on Polyelectrolyte Adsorption: Case Study of a Poly(Styrenesulfonate) Monolayer. Macromolecules 2011, 44 (6), 1707–1718. 10.1021/ma1026109.

(86). Qiao B; Sega M; Holm C An Atomistic Study of a Poly(Styrene Sulfonate)/ Poly(Diallyldimethylammonium) Bilayer: The Role of Surface Properties and Charge Reversal. Phys. Chem. Chem. Phys. 2011, 13 (36), 16336–16342. 10.1039/C1CP21777A. [PubMed: 21837314]

(87). Vögele M; Holm C; Smiatek J Coarse-Grained Simulations of Polyelectrolyte Complexes: MARTINI Models for Poly(Styrene Sulfonate) and Poly(Diallyldimethylammonium). J. Chem. Phys. 2015, 143 (24), 243151. 10.1063/1.4937805. [PubMed: 26723636]

(88). Jee A-Y; Curtis-Fisk JL; Granick S Nanoparticle Diffusion in Methycellulose Thermoreversible Association Polymer. Macromolecules 2014, 47 (16), 5793–5797.

(89). Skóra T; Vaghefikia F; Fitter J; Kondrat S Macromolecular Crowding: How Shape and Interactions Affect Diffusion. J. Phys. Chem. B 2020, 124 (35), 7537–7543. [PubMed: 32790396]

(90). Carr JK; Himes RD; Keung CH; Burden DL; Walhout PK Heterogeneous Translational Dynamics of Rhodamine B in Polyelectrolyte Multilayer Thin Films Observed by Single Molecule Microscopy. Langmuir 2009, 25 (14), 8330–8339. [PubMed: 19505126]

(91). Tauzin LJ; Shuang B; Kisley L; Mansur AP; Chen J; de Leon A; Advincula RC; Landes CF Charge-Dependent Transport Switching of Single Molecular Ions in a Weak Polyelectrolyte Multilayer. Langmuir 2014, 30 (28), 8391–8399. [PubMed: 24960617]

(92). Reznik C; Estillore N; Advincula RC; Landes CF Single Molecule Spectroscopy Reveals Heterogeneous Transport Mechanisms for Molecular Ions in a Polyelectrolyte Polymer Brush. J. Phys. Chem. B 2009, 113 (44), 14611–14618. 10.1021/jp906487j. [PubMed: 19813742]

(93). Reznik C; Darugar Q; Wheat A; Fulghum T; Advincula RC; Landes CF Single Ion Diffusive Transport within a Poly(Sterene Sulfonate) Polymer Brush Matrix Probed by Fluorescence Correlation Spectroscopy. J. Phys. Chem. B 2008, 112, 10890–10897. [PubMed: 18630854]

(94). Wang J; Wang W; Kollman PA; Case DA Automatic Atom Type and Bond Type Perception in Molecular Mechanical Calculations. J. Mol. Graph. Model. 2006, 25 (2), 247–260. [PubMed: 16458552]

(95). Wang J; Wolf RM; Caldwell JW; Kollman PA; Case DA Development and Testing of a General Amber Force Field. J. Comput. Chem. 2004, 25 (9), 1157–1174. [PubMed: 15116359]

(96). da Silva AWS; Vranken WF ACPYPE-Antechamber Python Parser Interface. BMC Res. Notes 2012, 5 (1), 367. [PubMed: 22824207]

(97). Eastman P; Swails J; Chodera JD; McGibbon RT; Zhao Y; Beauchamp KA; Wang L-P; Simmonett AC; Harrigan MP; Stern CD OpenMM 7: Rapid Development of High Performance Algorithms for Molecular Dynamics. PLoS Comput. Biol. 2017, 13 (7), e1005659. [PubMed: 28746339]

(98). Brooks BR; Brooks III CL; Mackerell AD Jr; Nilsson L; Petrella RJ; Roux B; Won Y; Archontis G; Bartels C; Boresch S CHARMM: The Biomolecular Simulation Program. J. Comput. Chem. 2009, 30 (10), 1545–1614. [PubMed: 19444816]

(99). Darden T; York D; Pedersen L Particle Mesh Ewald: An N· Log (N) Method for Ewald Sums in Large Systems. J. Chem. Phys. 1993, 98 (12), 10089–10092.

(100). Dünweg B; Kremer K Microscopic Verification of Dynamic Scaling in Dilute Polymer Solutions: A Molecular-Dynamics Simulation. Phys. Rev. Lett. 1991, 66 (23), 2996–2999. 10.1103/PhysRevLett.66.2996. [PubMed: 10043672]

(101). Yeh I-C; Hummer G System-Size Dependence of Diffusion Coefficients and Viscosities from Molecular Dynamics Simulations with Periodic Boundary Conditions. J. Phys. Chem. B 2004, 108 (40), 15873–15879. 10.1021/jp0477147.

(102). Venable RM; Hatcher E; Guvench O; MacKerell AD; Pastor RW Comparing Simulated and Experimental Translation and Rotation Constants: Range of Validity for Viscosity Scaling. J. Phys. Chem. B 2010, 114 (39), 12501–12507. 10.1021/jp105549s. [PubMed: 20831149]

(103). Yeh I-C; Hummer G Diffusion and Electrophoretic Mobility of Single-Stranded RNA from Molecular Dynamics Simulations. Biophys. J. 2004, 86 (2), 681–689. [PubMed: 14747307]

(104). Mamatkulov S; Schwierz N Force Fields for Monovalent and Divalent Metal Cations in TIP3P Water Based on Thermodynamic and Kinetic Properties. J. Chem. Phys. 2018, 148 (7), 074504. [PubMed: 29471634]

(105). Sajadi F; Rowley CN Simulations of Lipid Bilayers Using the CHARMM36 Force Field with the TIP3P-FB and TIP4P-FB Water Models. PeerJ 2018, 6, e5472. [PubMed: 30128211]

(106). Hiemenz PC Polymer Chemistry: The Basic Concepts, Marcel Dekker. Inc N. Y. Basel 1984, 51–52.

(107). Shrake A; Rupley JA Environment and Exposure to Solvent of Protein Atoms. Lysozyme and Insulin. J. Mol. Biol. 1973, 79 (2), 351–371. [PubMed: 4760134]

(108). Lee B; Richards FM The Interpretation of Protein Structures: Estimation of Static Accessibility. J. Mol. Biol. 1971, 55 (3), 379–IN4. [PubMed: 5551392]

(109). Feig M; Karanicolas J; Brooks III CL MMTSB Tool Set: Enhanced Sampling and Multiscale Modeling Methods for Applications in Structural Biology. J. Mol. Graph. Model. 2004, 22 (5), 377–395. [PubMed: 15099834]

(110). Yamakawa H; Yoshizaki T Helical Wormlike Chains in Polymer Solutions; Springer, 1997; Vol. 1.

(111). Cifra P Differences and Limits in Estimates of Persistence Length for Semi-Flexible Macromolecules. Polymer 2004, 45 (17), 5995–6002.

(112). Yashiro J; Norisuye T Excluded-Volume Effects on the Chain Dimensions and Transport Coefficients of Sodium Poly(Styrene Sulfonate) in Aqueous Sodium Chloride. J. Polym. Sci. Part B Polym. Phys. 2002, 40 (23), 2728–2735. 10.1002/polb.10324.

(113). Gendron PO; Avaltroni F; Wilkinson KJ Diffusion Coefficients of Several Rhodamine Derivatives as Determined by Pulsed Field Gradient-Nuclear Magnetic Resonance and Fluorescence Correlation Spectroscopy. J. Fluoresc. 2008, 18 (6), 1093–1101. [PubMed: 18431548]

(114). Wang F; Shi Y; Luo S; Chen Y; Zhao J Conformational Transition of Poly (N-Isopropylacrylamide) Single Chains in Its Cononsolvency Process: A Study by Fluorescence Correlation Spectroscopy and Scaling Analysis. Macromolecules 2012, 45 (22), 9196–9204.

(115). Ozbek H; Fair JA; Phillips SL Viscosity of Aqueous Sodium Chloride Solutions From 0–150°C; Lawrence Berkeley National Lab.(LBNL), Berkeley, CA (United States), 1977.

(116). Vilaseca E; Isvoran A; Madurga S; Pastor I; Garcés JL; Mas F New Insights into Diffusion in 3D Crowded Media by Monte Carlo Simulations: Effect of Size, Mobility and Spatial Distribution of Obstacles. Phys. Chem. Chem. Phys. 2011, 13 (16), 7396–7407. [PubMed: 21412541]

(117). Vilaseca E; Pastor I; Isvoran A; Madurga S; Garcés J-L; Mas F Diffusion in Macromolecular Crowded Media: Monte Carlo Simulation of Obstructed Diffusion vs. FRAP Experiments. Theor. Chem. Acc. 2011, 128 (4–6), 795–805. 10.1007/s00214-010-0840-5.

(118). Pal SK; Peon J; Zewail AH Biological Water at the Protein Surface: Dynamical Solvation Probed Directly with Femtosecond Resolution. Proc. Natl. Acad. Sci. 2002, 99 (4), 1763–1768. [PubMed: 11842218]

(119). Zhong D; Pal SK; Zewail AH Biological Water: A Critique. Chem. Phys. Lett. 2011, 503 (1–3), 1–11.

(120). Bagchi B Water in Biological and Chemical Processes: From Structure and Dynamics to Function; Cambridge University Press, 2013.

(121). Wang P; Yu I; Feig M; Sugita Y Influence of Protein Crowder Size on Hydration Structure and Dynamics in Macromolecular Crowding. Chem. Phys. Lett. 2017, 671, 63–70. 10.1016/j.cplett.2017.01.012.

(122). Ellery AJ; Baker RE; McCue SW; Simpson MJ Modeling Transport through an Environment Crowded by a Mixture of Obstacles of Different Shapes and Sizes. Phys. Stat. Mech. Its Appl. 2016, 449, 74–84.

(123). Ma Y; Luo K Anomalous and Normal Diffusion of Tracers in Crowded Environments: Effect of Size Disparity between Tracer and Crowders. Chin. J. Chem. Phys. 2017, 30 (2), 147–152. 10.1063/1674-0068/30/cjcp1609184.

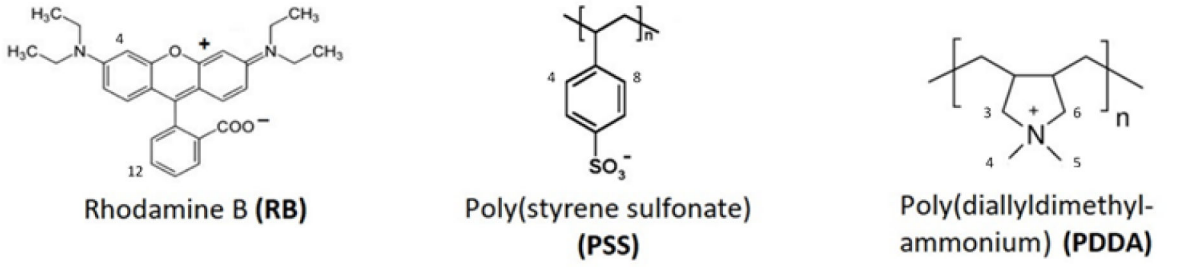

Figure 1.
Molecular structures of RB zwitterion, PSS, and PDDA. (Numbers denote carbon atoms mentioned in the text.)

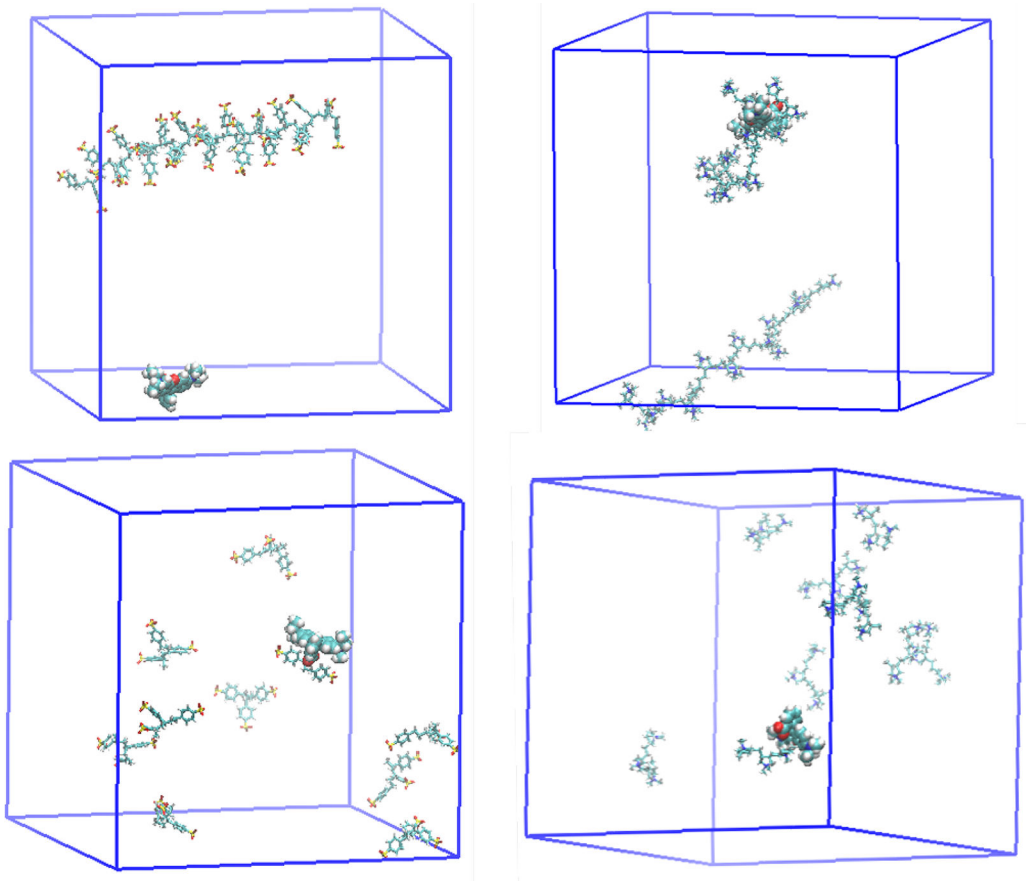

Figure 2.

Snapshots from each of the four simulated PE systems (see Table 1). Each system has one RB molecule and various PE molecules in a 0.1 M NaCl aqueous solution (water and salt not shown). The top row shows longer chain PEs: 30-mer chain of PSS (*top left*) and two 15-mer PDDA chains (*top right*), and the bottom row shows 10 trimers: PSS (*bottom left*) and PDDA (*bottom right*). Association of the RB and a PDDA 15-mer is evident in the upper right.

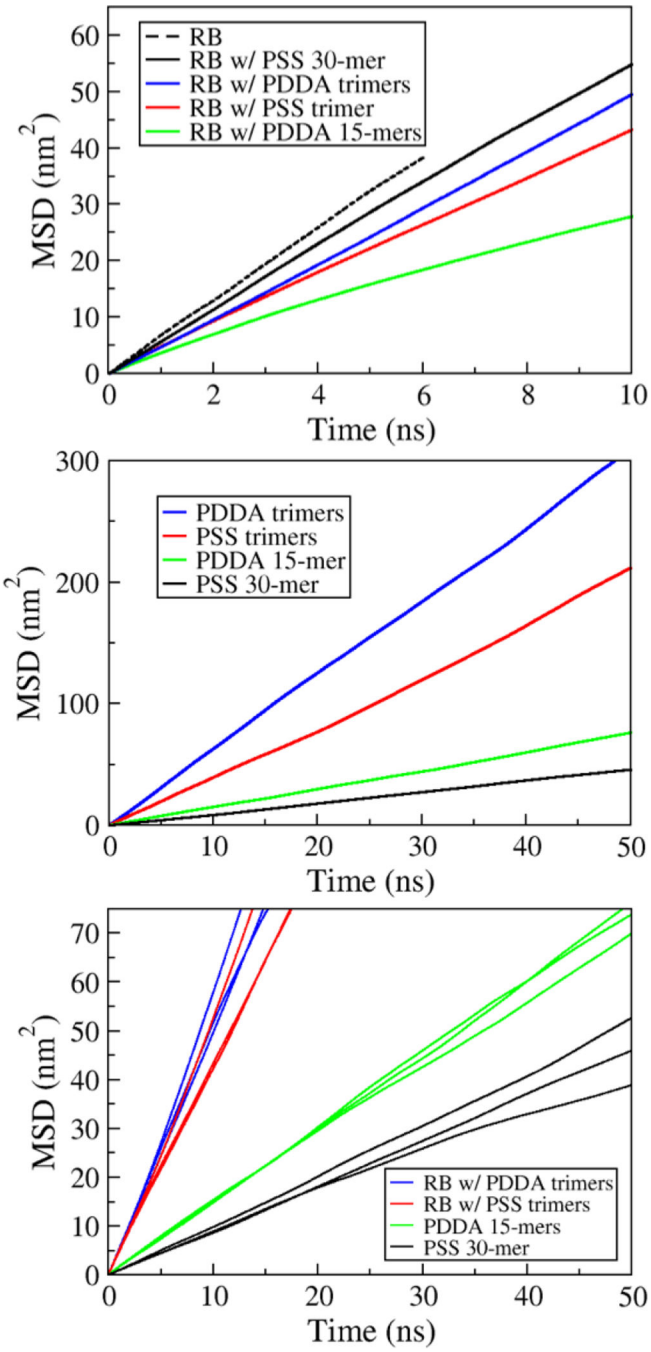

Figure 3.

Mean square displacement (MSD) of various molecules plotted vs. the time lag, **τ**, from eq 1. Each MSD plot from one of the simulated systems is generated from one of the three triplicate 1-μs runs. *Top*: MSD of RB in all the simulated systems, including PE-free water (top plot) and the four PE solutions (all include 0.1 M NaCl). *Middle*: MSD of each of the four simulated PE molecules. *Bottom*: A visual depiction of the reproducibility of the diffusion simulations; MSDs from each of the three triplicate runs is shown for four systems.

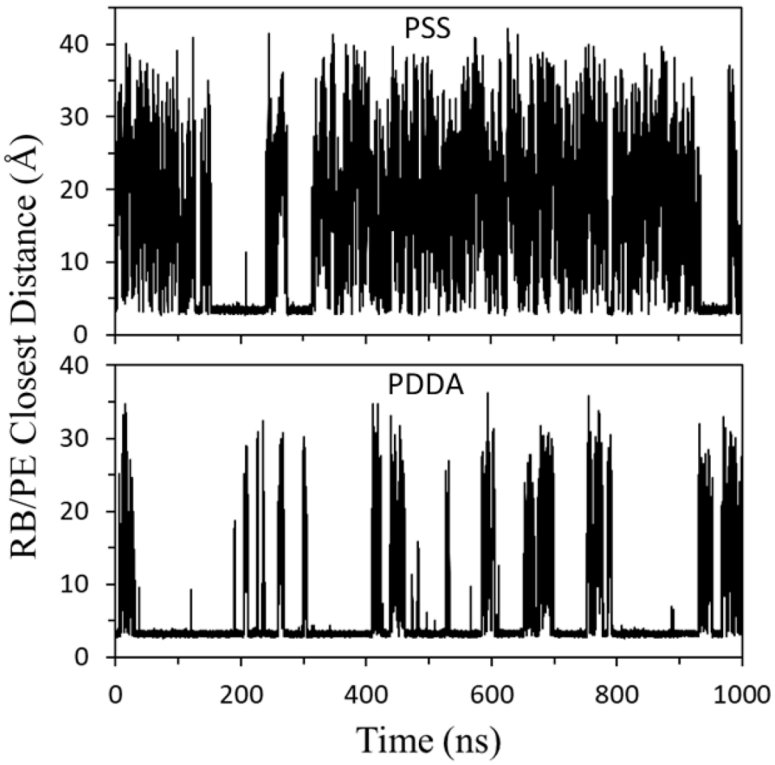

Figure 4.

Plots of the closest heavy-atom distance at each timestep between RB and PSS 30-mer (top) and PDDA 15-mers (bottom). It is clear that long duration associations with both polymers occur with a separation under 5 Å.

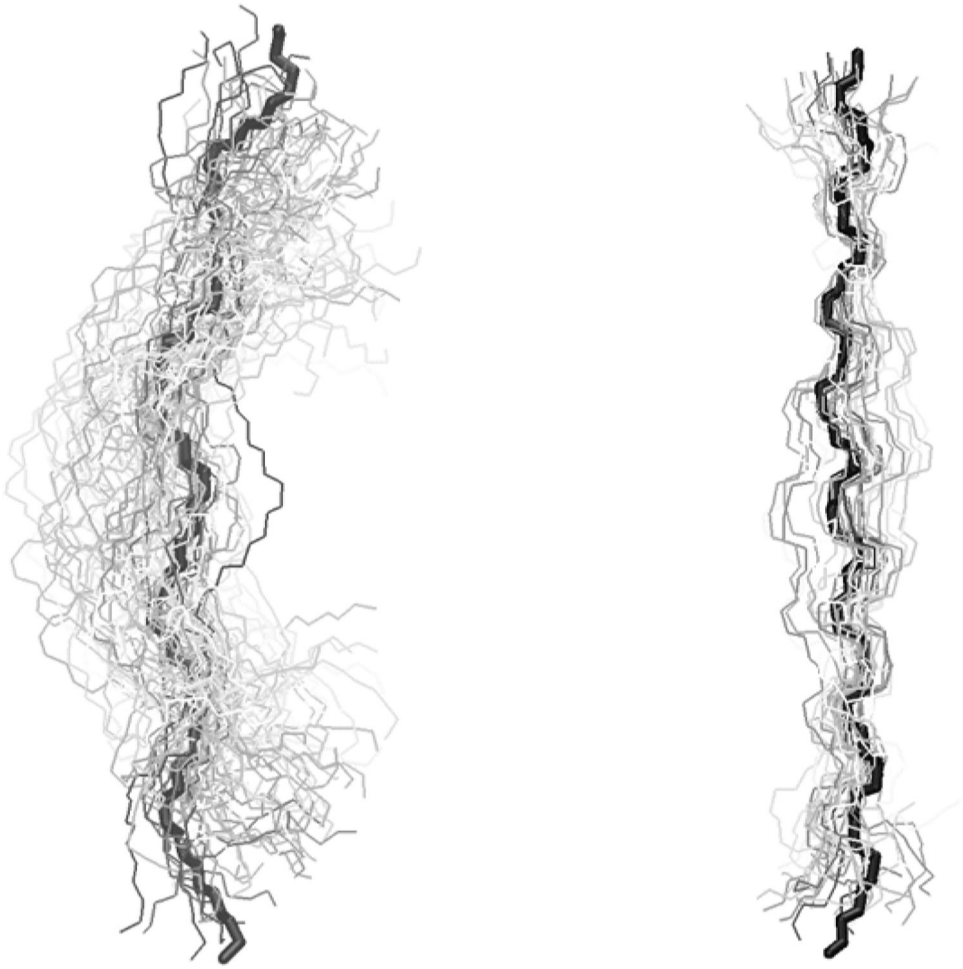

Figure 5.

Depiction of conformational sampling during the simulations by the PDDA 15-mer (left) and PSS 30-mer (right). Only heavy atoms are included, with the color going from black to white for decreasing sampling.

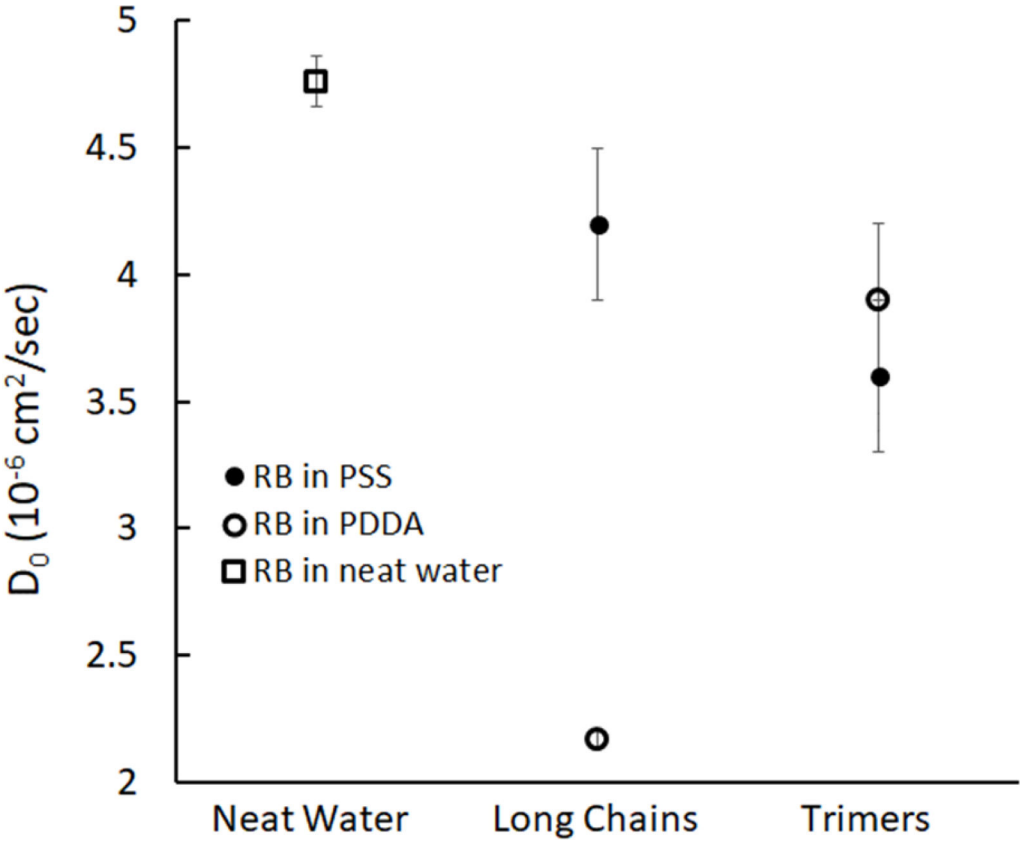

Figure 6.

A visual depiction of the key D_0 data points from Table 4, including D_0 for RB in PE-free (neat) water, in long-chain solutions (PSS 30-mer and PDDA 15-mer), and in PSS and PDDA trimer solutions. D_0 for RB in neat water is an average of all three NaCl concentrations, hence the smaller error bar.

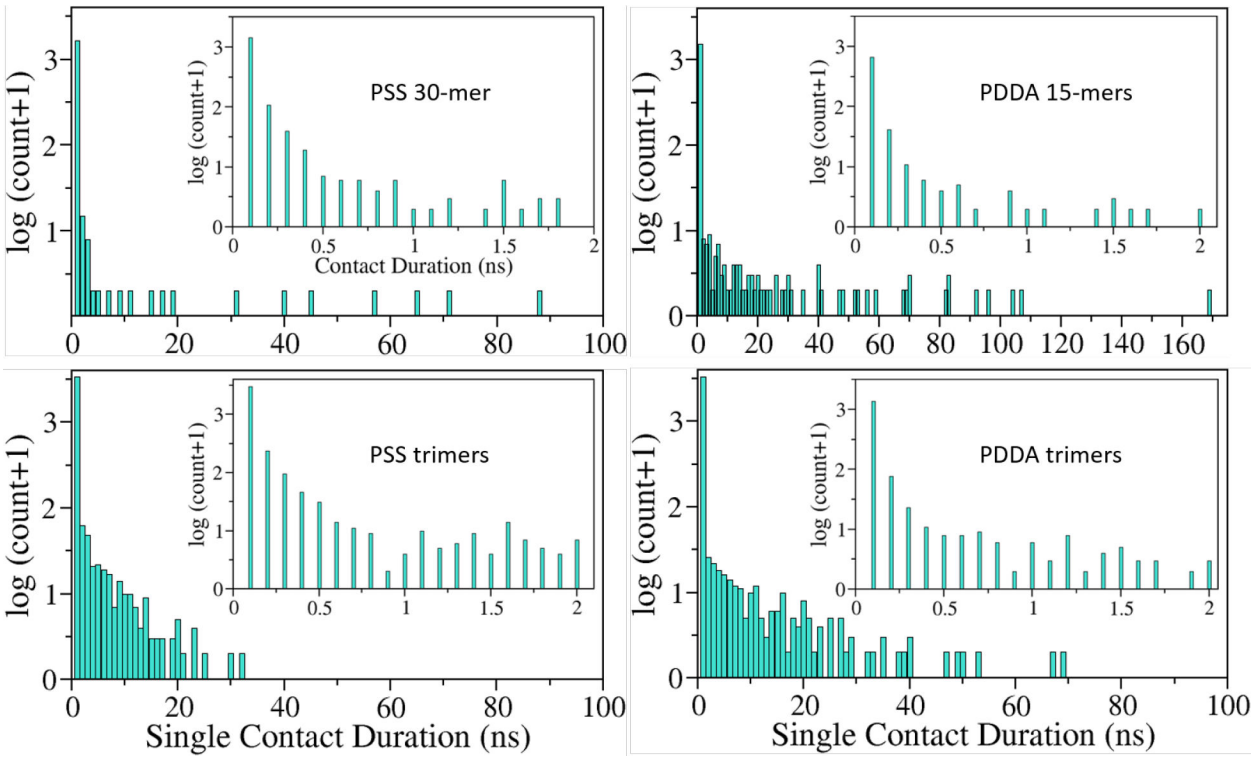

Figure 7.

Histograms depicting the duration of individual RB/PE contact events (bin width = 1 ns) compiled from all three runs for each simulation system. A log scale is used because of the dominance of contact durations ≤ 1 ns. A one-time event has a y-axis value of 0.301 (log 2). The insets for each plot are similar histograms with 0.1 ns bin widths, plotted to 2 ns. The insets for the four systems are quite similar, showing that the vast majority of contact durations ≤ 1 ns are actually ≤ 0.1 ns (100 ps) and can be attributed to short-term, non-associative encounters.

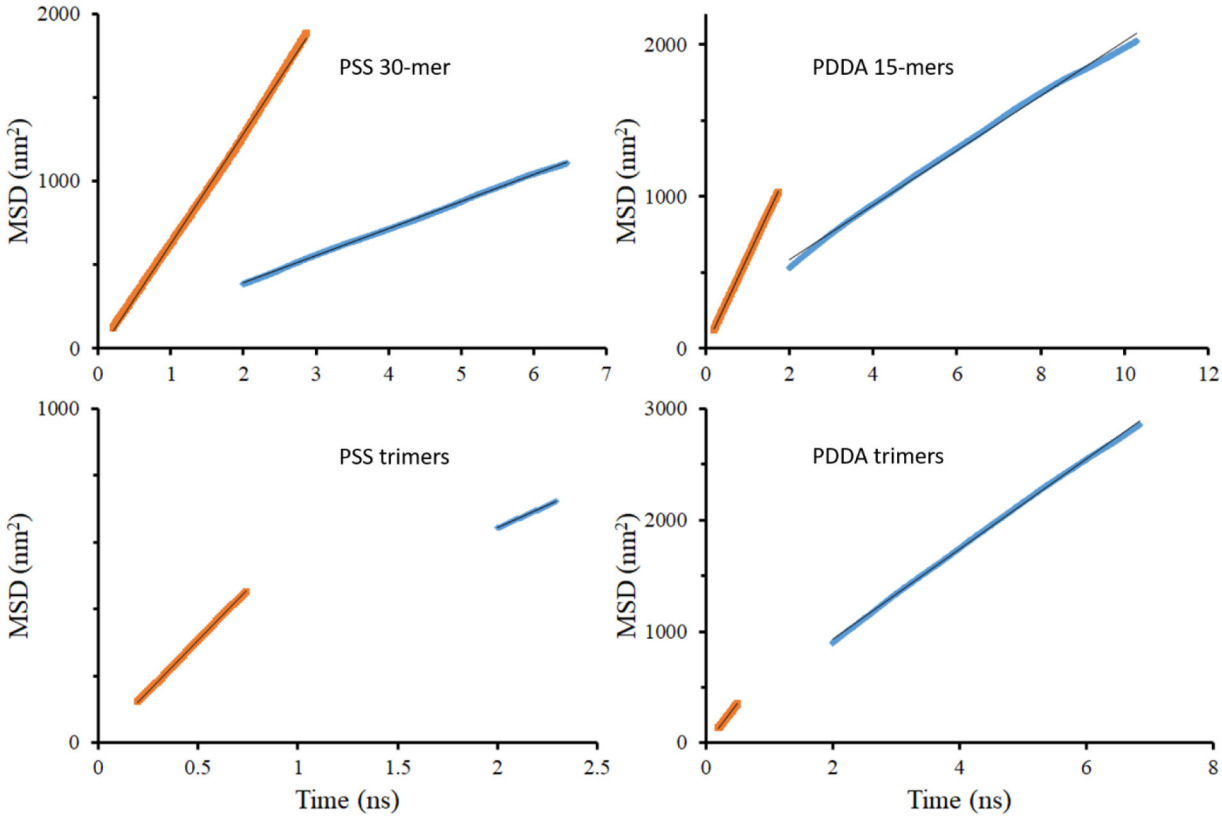

Figure 8.

Representative plots of RB 'contact' (blue) and 'free' (orange) mean-square-displacements (MSD) in each PE system. For each plot, separate PE-contact and PE-free periods of RB diffusion were isolated from the 1 μs trajectories, from which separate MSDs were compiled. Linear fits (black lines) were made to determine D_{free} and D_{bound} in each system. For each MSD, data was fit to 10% of the total time length. For the contact MSDs, the first 2 ns were eliminated, and for the free MSDs, only the first 0.2 ns was eliminated due to the limited length of those MSDs.

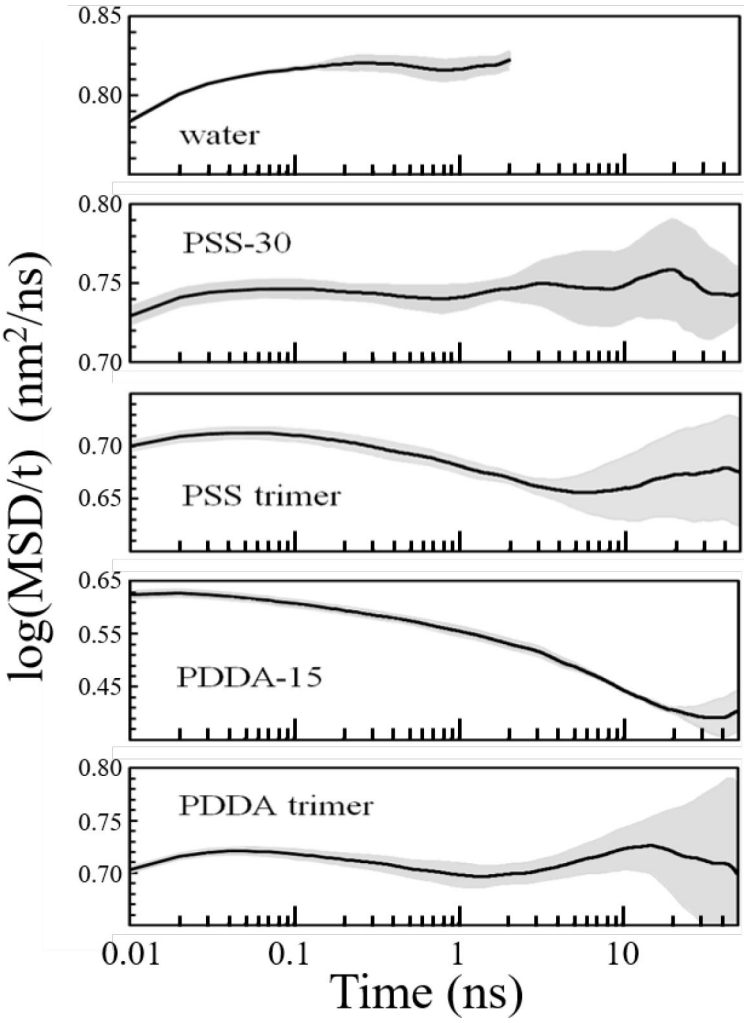

Figure 9.

Anomalous indicator plots for RB diffusion in all systems studied. All panels depict an average of the three independent trajectories for each system and the standard error of the average (grey). The top panel is RB diffusion in aqueous 100 mM NaCl.

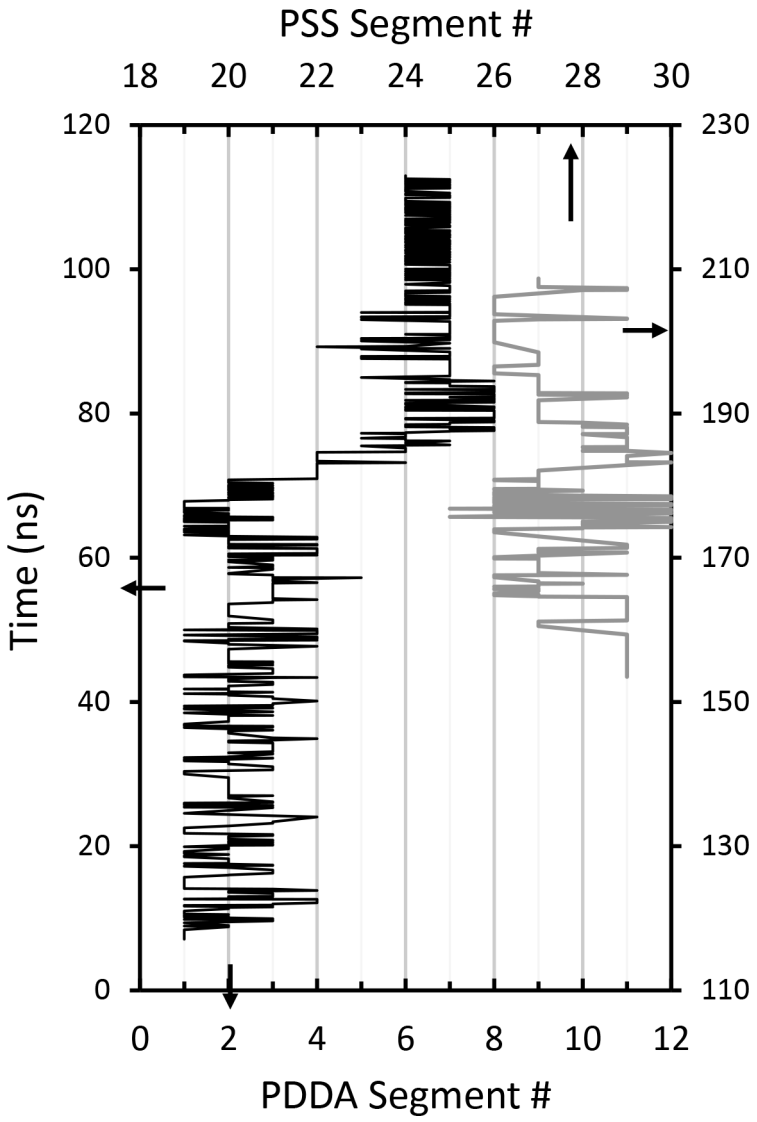

Figure 10.

Motion of a single RB atom along the polymer backbone for two association events. The left black plot is from run 1 of RB with PDDA 15-mers, and the right gray plot is from run1 of RB with PSS 30-mer. The first lengthy association event from each run was arbitrarily selected to be plotted. In the events plotted here, the monitored RB atom contacts eight different PDDA repeat unit segments and six different PSS segments.

Table 1.

Simulated systems performed using CHARMM/OpenMM.

I[a]	DP[b]	N[c]	Duration[d] (ns)	L (Å)[e]	c_S [f] (M)	N_{water} [g]
PSS	30	1	1000	78.00	0.10	15263
	30	1	1000	78.00	0.10	15265
	30	1	1000	78.00	0.10	15271
	3	10	1000	78.00	0.10	15210
	3	10	1000	78.00	0.10	15211
	3	10	1000	78.00	0.10	15209
PDDA	15	2	1000	78.00	0.10	15176
	15	2	1000	78.00	0.10	15172
	15	2	1000	78.00	0.10	15200
	3	10	1000	78.00	0.10	15156
	3	10	1000	78.00	0.10	15183
	3	10	1000	78.00	0.10	15164

[a] Identity of polymer

[b] Degree of polymerization of polyelectrolytes

[c] Number of polymer chains

[d] Duration of the simulation

[e] Edge length of the cubic solvation box

[f] Concentration of salt (NaCl) in the solution

[g] Total number of water molecules in the boxes

Table 2.

Three control systems of RB diffusing in aqueous solutions without polyelectrolyte

t[b] (ns)	L (Å)[b]	cs [c] (M)	N_{water} [d]
300	78.00	0	15649
300	78.00	0.050	15621
300	78.00	0.10	15593

[a] Total duration of the simulations

[b] Dimension of the cubic box

[c] Concentration of salt (NaCl) in the solution

[d] Total number of water molecules in the boxes

Table 3.

Size characterizations of polyelectrolytes in the simulated systems.

	r_{rms} [a] (Å)	$R_{g,rmS}$ [b] (Å)	SASA [c] (10^4 Å^2)
PSS 30-mer	54 ± 2	17.8 ± 0.3	5.03 ± 0.08
PSS trimer	5.5 ± 0.3	4.90 ± 0.12	4.93 ± 0.03
PDDA 15-mer	45 ± 5	16.2 ± 1.0	5.140 ± 0.015
PDDA trimer	10.2 ± 1.0	5.10 ± 0.12	4.94 ± 0.03

All values are averages from three runs.

[a] Average root-mean-square end-to-end distance, calculated between the two carbon end atoms.

[b] Root-mean-square radius of gyration.

[c] Solvent accessible surface area. Reported errors are the estimated standard errors of the mean.

Table 4.

Diffusion coefficients of RB and polyelectrolytes from simulations

	D_{MD} (10^{-6} cm^2/s)	$D_{0,TIP3P}$ (10^{-6} cm^2/s)	D_0 (10^{-6} cm^2/s)	*Experiment/Theory* (10^{-6} cm^2/s)
PSS 30-mer	1.55 ± 0.05	3.54 ± 0.05	1.27 ± 0.02	1.4[a]
PSS trimer	6.90 ± 0.03	8.88 ± 0.03	3.18 ± 0.10	
PDDA 15-mer	2.46 ± 0.02	4.45 ± 0.02	1.592 ± 0.008	~1.4[b]
PDDA trimer	10.4 ± 0.3	12.4 ± 0.3	4.44 ± 0.10	
RB (0 M NaCl)	11.0 ± 0.9	13.0 ± 0.9	4.6 ± 0.3	4.7[c]
RB (0.05 M NaCl)	10.8 ± 0.5	12.8 ± 0.5	4.6 ± 0.2	
RB (0.1 M NaCl)	11.77 ± 0.14	13.76 ± 0.14	4.92 ± 0.05	
RB (w/PSS 30-mer)	9.7 ± 0.8	11.7 ± 0.8	4.2 ± 0.3	3.5[d]
RB (w/PSS trimers)	8.0 ± 0.9	10.0 ± 0.9	3.6 ± 0.3	
RB (w/PDDA 15-mers)	4.00 ± 0.09	5.98 ± 0.09	2.14 ± 0.03	3.8[d]
RB (w/PDDA trimers)	9.0 ± 0.9	11.0 ± 0.9	3.9 ± 0.3	

The various diffusion coefficients heading the first three data columns are as described in the text. Reported D_{MD} values are from averaging linear fits of the MSD vs. time plots from three independent simulations of each system. The reported error is the estimated standard error of the mean of the three fits. The last column provides predictions or results based on experiment.

[a] Prediction based on data from Yashiro et al.[112] (see SI for details).

[b] Prediction based on similar estimated R_g values from Marcelo et al.[28] to PSS 30-mer (see SI for details).

[c] Experimental value from Gendron et al.[113]

[d] Prediction based only on wt% of PE from Zhang et al.[34] data, with no distinction between trimers and longer chains.

Table 5.

Contact analysis of RB with polyelectrolytes

	Cumulative contact duration (ns)	Cumulative contact duration of events > 0.5 ns	Total # of separate contacts	# of events > 0.5 ns	Average contact duration of events > 0.5 ns	Longest contact duration (ns)
PSS 30-mer						
1	223.3	201.6	567	20	10.1	56.1
2	204.9	181.5	527	15	12.1	87.5
3	170.2	144.0	575	19	7.6	64.7
Avg.	**199 ± 20**	**176 ± 20**	**556 ± 15**	**18 ± 2**	**9.9 ± 1.3**	**69 ± 9**
PSS trimers						
1	629.5	576.5	1115	99	5.82	39.7
2	534.8	479.0	1277	89	5.38	21.9
3	565.7	504.8	1301	105	4.81	22.9
Avg.	**577 ± 30**	**520 ± 30**	**1231± 60**	**98 ± 5**	**5.3 ± 0.3**	**28 ± 6**
PDDA 15-mers						
1	830.2	822.9	220	30	27.4	106.1
2	778.8	768.3	357	36	21.3	169.1
3	753.6	741.1	371	34	21.8	103.4
Avg.	**787 ± 20**	**777 ± 20**	**316 ± 50**	**33 ± 2**	**24 ± 2**	**126 ± 20**
PDDA trimers						
1	802.0	781.5	657	82	9.53	66.0
2	830.2	814.0	497	69	11.8	52.2
3	811.2	793.4	564	84	9.45	68.4
Avg.	**814 ± 8**	**796 ± 9**	**573 ± 50**	**78 ± 5**	**10.3 ± 0.8**	**62 ± 5**

Results are shown for each of three independent 1 μs trajectories for each system, along with their averages. Contact is defined as the closest heavy atoms of RB and the PE being < 0.5 nm apart. Reported errors are the estimated standard error of the means.

Table 6.

Two-component RB diffusion model

	PSS 30-mer	PSS trimers	PDDA 15-mers	PDDA trimers
f_{bound}	0.18 ± 0.02	0.52 ± 0.03	0.78 ± 0.02	0.796 ± 0.009
f_{free}	0.82 ± 0.02	0.48 ± 0.03	0.22 ± 0.02	0.204 ± 0.009
D_{bound} (10^{-6} cm^2/s)	1.83 ± 0.09	2.5 ± 0.2	1.72 ± 0.04	3.45 ± 0.16
D_{free} (10^{-6} Cm^2/s)	4.5 ± 0.1	4.27 ± 0.13	4.19 ± 0.05	4.6 ± 0.3
D_{eff} (10^{-6} cm^2/s)	4.00 ± 0.12	3.33 ± 0.2	2.27 ± 0.11	3.68 ± 0.15
D_{eff}* (10^{-6} cm^2/s)	4.19 ± 0.13	3.56 ± 0.2	2.38 ± 0.13	3.70 ± 0.14
$D_{0,RB}$ (10^{-6} cm^2/s)	4.2 ± 0.3	3.6 ± 0.3	2.14 ± 0.03	3.9 ± 0.3
$D_{0,RB}/D_{eff}$	1.04 ± 0.08	1.07 ± 0.11	0.94 ± 0.05	1.08 ± 0.10
$D_{0,RB}/D_{eff}$*	1.00 ± 0.08	1.00 ± 0.10	0.90 ± 0.05	1.06 ± 0.10

Reported errors are the estimated standard error of the means from three runs. D_{eff}* is calculated using a larger value of D_{free} derived from RB simulations in PE-free water.

Table 7.

Atoms involved in closest contacts during RB/PE associations (top two for each molecule)

	PSS 30-mer	PSS trimers	PDDA 15-mer	PDDA trimers
PE contact atom	$C_{4,8}$ (32.4%)	$C_{4,8}$ (32.2%)	$C_{4,5}$ (40.7%)	$C_{4,5}$ (40.0%)
	O^a (29.4%)	O^a (17.4%)	$C_{3,6}$ (33.6%)	$C_{3,6}$ (33.3%)
RB contact atom	O^b (27.9%)	O^b (29.1%)	O^b (79.5%)	O^b (76.9%)
	$C_{meth}{}^c$ (20.8%)	$C_{meth}{}^c$ (17.3%)	C_4 (4.7%)	C_4 (5.3%)

Numerical subscripts on the carbons refer to designations in Figure 1 and in Tables S1–S3.

[a]Refers to any of the three sulfonate oxygens

[b]Refers to the combined two carboxylate oxygens and the ether (xantheynyl) oxygen. The relative frequency of closest contact among these three is roughly 3:3:1

[c]Refers to the combined four equivalent methyl carbons at the end of the ethyl chains.

Table 8.

RB sampling of PE segments during association (cumulative from three runs)

	Event Duration (ns)				Event Duration (ns)		
	0.05–0.5	**0.5 – 5**	**> 5**		**0.05–0.5**	**0.5 – 5**	**> 5**
PDDA 15-mers				PSS 30-mer			
# events	165	31	69		420	42	13
total time (ns)	18.2	63.0	2269		51.1	57.7	470
time/event (ns)	0.110	2.03	32.9		0.122	1.37	36.1
<# PE segments>	1.11	2.48	5.90		1.12	2.02	5.85
# PE switches	4	95	8890		17	48	424
time/switch (ns)	4.54	0.663	0.255		3.00	1.20	1.11
PDDA trimers				PSS trimers			
# events	284	104	131		986	187	108
total time (ns)	34.0	232	2157		126	394	1168
time/event (ns)	0.120	2.23	16.5		0.128	2.10	10.8
<# PE segments>	1.08	2.40	2.99		1.04	2.36	2.97
# PE switches	5	442	6606		7	269	961
time/switch (ns)	6.79	0.524	0.327		18.0	1.46	1.22